

# INVESTIGATION OF LEAD-FREE PEROVSKITE MASNI3 BASED SOLAR CELLS USING SCAPS SIMULATION

LUQMAN HAKIM BIN ZAINUL ABIDDIN



UNIVERSITI TEKNIKAL MALAYSIA MELAKA

**INVESTIGATION OF LEAD-FREE PEROVSKITE MASNI3  
BASED SOLAR CELLS USING SCAPS SIMULATION**

**LUQMAN HAKIM BIN ZAINUL ABIDDIN**

**This report is submitted in partial fulfilment of the requirements  
for the degree of Bachelor of Electronic Engineering with Honours**

**Faculty of Electronic and Computer Technology and Engineering  
Universiti Teknikal Malaysia Melaka**

UNIVERSITI TEKNIKAL MALAYSIA MELAKA

**2024**

**BORANG PENGESAHAN STATUS LAPORAN  
PROJEK SARJANA MUDA II**

Tajuk Projek : Investigation of Lead-Free Perovskite MASnI3 Based  
Solar Cells Using SCAPS Simulation  
Sesi Pengajian : 2023/2024

Saya LUQMAN HAKIM BIN ZAINUL ABIDDIN mengaku membenarkan laporan Projek Sarjana Muda ini disimpan di Perpustakaan dengan syarat-syarat kegunaan seperti berikut:

1. Laporan adalah hakmilik Universiti Teknikal Malaysia Melaka.
2. Perpustakaan dibenarkan membuat salinan untuk tujuan pengajian sahaja.
3. Perpustakaan dibenarkan membuat salinan laporan ini sebagai bahan pertukaran antara institusi pengajian tinggi.
4. Sila tandakan (✓):

**SULIT\***

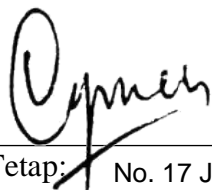
(Mengandungi maklumat yang berdarjah keselamatan atau kepentingan Malaysia seperti yang termaktub di dalam AKTA RAHSIA RASMI 1972)

**TERHAD\***

(Mengandungi maklumat terhad yang telah ditentukan oleh organisasi/badan di mana penyelidikan dijalankan.)

**TIDAK TERHAD**

Disahkan oleh:



(COP DAN



PENYELIA)

Alamat Tetap: No. 17 Jalan Masjid Sultan, 42/KS13 Kg. Perigi Nenas, 42920, Pulau Indah, Selangor

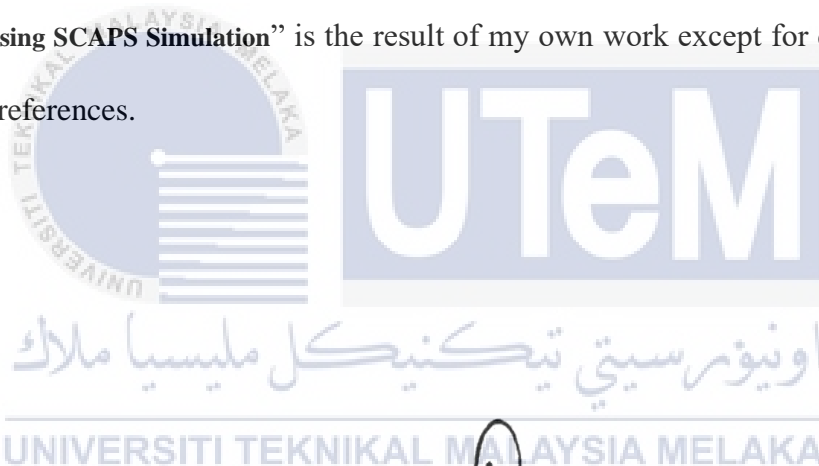
**SITI AISAH BINTI MAT JUNOS @ YUNUS**  
Pensyarah  
Fakulti Teknologi Dan Kejuruteraan Elektronik Dan Komputer (FTKEK)  
Universiti Teknikal Malaysia Melaka (UTeM)

Tarikh : 22 January 2024 Tarikh : 22 January 2024

\*CATATAN: Jika laporan ini SULIT atau TERHAD, sila lampirkan surat daripada pihak berkuasa/organisasi berkenaan dengan menyatakan sekali tempoh laporan ini perlu dikelaskan sebagai SULIT atau TERHAD.

## DECLARATION

I declare that this report entitled “**Investigation of Lead-Free Perovskite MASnI<sub>3</sub> Based Solar Cells Using SCAPS Simulation**” is the result of my own work except for quotes as cited in the references.



Signature : .....

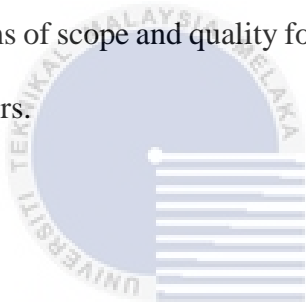
A handwritten signature in black ink, appearing to read 'Luqman', is written over the dotted line of the signature field.

Author : Luqman Hakim Bin Zainul Abiddin

Date : 22 Jan., 24

# APPROVAL

I hereby declare that I have read this thesis and in my opinion this thesis is sufficient in terms of scope and quality for the award of Bachelor of Electronic Engineering with Honours.



اونيوه ستيك ايسا بinti ملوك  
UNIVERSITI TEKNIKAL MALAYSIA MELAKA

Signature : ..

Supervisor Name : ..  
SITI AISAH BINTI MAT JUNOS @ YUNUS  
Pensyarah  
Fakulti Teknologi Dan Kejuruteraan Elektronik Dan Komputer (FTKEK)  
Universiti Teknikal Malaysia Melaka (UTeM)

Date : 23 January 2024 ..

## DEDICATION

My heartfelt gratitude goes to my supportive parents, family and dear friends who have stood by me through the various challenges of completing this dissertation and have offered me unwavering support through both triumphs and setbacks. In addition, this work is dedicated to my supervisor, whose guidance emphasized that mastery is not the priority. Rather, hard work and passion are the cornerstones for the successful completion of a project.

UNIVERSITI TEKNIKAL MALAYSIA MELAKA

## ABSTRACT

Perovskite solar cells (PSC) have attracted significant attention in recent years due to their rapid advances in power conversion efficiency (PCE), cost-effectiveness, and simplified synthesis process. However, challenges related to perovskite stability and the use of toxic lead as a component are hindering the widespread adoption of perovskite-based solar cells. This study focuses on the optimization of the  $\text{MASnI}_3$ -based absorber layer in the PSC structure, including the electron transport layer (ETL) and hole transport layer (HTL), by using SCAPs software device simulation. This study investigates the influence of various parameters on the performance of solar cells. The simulation results show that each layer plays a crucial role in determining the overall performance of PSCs and that optimizing these layers significantly increases their efficiency. The optimized structure for lead-free PSC using  $\text{TiO}_2$  as ETL shows remarkable PSC performance with parameters such as  $J_{sc}$  (33.8766  $\text{mA}/\text{cm}^2$ ),  $V_{oc}$  (1.1419 V), FF (88.95) and PCE (34.41%). Meanwhile, the optimized structure for lead-free PSC using  $\text{SnO}_2$  as ETL shows exceptional performance in perovskite solar cells (PSCs), with parameters such as  $J_{sc}$  (33.6529  $\text{mA}/\text{cm}^2$ ),  $V_{oc}$  (1.1414 V), FF (89.02) and PCE (34.19%) due to comprehensive parameter analysis.

## ABSTRAK

*Sel Surya Perovskite (PSC) telah mendapat perhatian penting dalam beberapa tahun kebelakangan ini kerana kemajuan pesatnya dalam kecekapan penukaran kuasa (PCE), keberkesanan kos dan proses sintesis yang amat mudah. Walau bagaimanapun, cabaran berkaitan dengan kestabilan perovskit dan penggunaan plumbum toksik sebagai komponen menghalang penggunaan meluas sel suria berasaskan perovskit. Kajian ini memberi tumpuan terhadap mengoptimumkan lapisan penyerap berasaskan  $\text{MASnI}_3$  dalam struktur PSC, termasuk Lapisan Pengangkutan Elektron (ETL), dan Lapisan Pengangkutan Lubang (HTL), melalui penggunaan simulasi peranti perisian SCAPs, kajian ini mengkaji pengaruh parameter yang berbeza terhadap prestasi sel suria. Penyelidikan juga meneroka kesan pelbagai jenis bahan yang digunakan untuk lapisan ETL. Keputusan simulasi mendedahkan bahawa setiap lapisan memainkan peranan penting dalam menentukan prestasi keseluruhan PSC, dan mengoptimumkan lapisan ini dengan ketara meningkatkan kecekapannya. Struktur yang menggunakan  $\text{TiO}_2$  sebagai ETL dioptimumkan dan menunjukkan prestasi PSC yang mengagumkan dengan parameter termasuk  $J_{sc}$  (33.8766  $\text{mA}/\text{cm}^2$ ),  $V_{oc}$  (1.1419 V), FF (88.95), dan PCE (34.41%) hasil daripada analisis parametrik yang komprehensif. Selain itu, struktur yang menggunakan  $\text{SnO}_2$  sebagai ETL juga menunjukkan prestasi yang baik dengan parameter  $J_{sc}$  (33.6529  $\text{mA}/\text{cm}^2$ ),  $V_{oc}$  (1.1414 V), FF (89.02), dan PCE (34.19%).*



## ACKNOWLEDGEMENTS

I would like to express my sincere thanks to my supervisor, Mdm. Siti Aisah Binti Junos @ Yunus, for her invaluable guidance and support throughout the project. Her expertise and commitment to teaching made it an honor to work under her supervision. I was grateful for her patience in answering my questions and providing constructive feedback on my project. Your guidance and encouragement helped me understand the project better and complete it successfully. I would also like to thank my family for their constant love and support. Their prayers and encouragement kept me motivated throughout the project. I was especially grateful to my parents for their unwavering support and for teaching me the importance of hard work and determination. I would also like to thank my friends and project partners for their support and encouragement. Your ideas and suggestions helped me improve my work and complete the project successfully. Finally, I would like to thank everyone who supported me directly or indirectly during this project, including the staff and faculty of the Faculty of Electronic and Computer Engineering, Universiti Teknikal Malaysia Melaka and all other people who helped me in any way. Your support and encouragement were crucial for me to achieve my goals and successfully complete this project.

## TABLE OF CONTENTS

<b>Declaration</b>	
<b>Approval</b>	
<b>Dedication</b>	<b>i</b>
<b>Abstract</b>	<b>ii</b>
<b>Abstrak</b>	<b>iii</b>
<b>Acknowledgements</b>	<b>iv</b>
<b>Table of Contents</b>	<b>v</b>
<b>List of Figures</b>	<b>ix</b>
<b>List of Tables</b>	<b>xi</b>
<b>List of Symbols and Abbreviations</b>	<b>xiii</b>
<b>CHAPTER 1: INTRODUCTION</b>	<b>1</b>
<b>1.1 Background</b>	<b>1</b>
<b>1.2 Problem Statement</b>	<b>2</b>
<b>1.3 Project Objectives</b>	<b>3</b>

<b>1.4</b>	<b>Project Scope</b>	<b>3</b>
<b>1.5</b>	<b>Importance of Study</b>	<b>3</b>
<b>1.6</b>	<b>Thesis Outline</b>	<b>4</b>
<b>CHAPTER 2: BACKGROUND STUDY</b>		<b>6</b>
<b>2.1</b>	<b>Photovoltaic (PV)</b>	<b>7</b>
<b>2.2</b>	<b>Generation of Solar Cell</b>	<b>8</b>
<b>2.3</b>	<b>Perovskite Solar cell</b>	<b>11</b>
<b>2.4</b>	<b>Key Parameter of Solar Cell's interest</b>	<b>13</b>
<b>2.4.1</b>	<b>Voltage Open Circuit (Voc)</b>	<b>13</b>
<b>2.4.2</b>	<b>Current Short Circuit (Jsc)</b>	<b>14</b>
<b>2.4.3</b>	<b>Fill Factor (FF)</b>	<b>15</b>
<b>2.4.4</b>	<b>Power Conversion Efficiency (PCE)</b>	<b>16</b>
<b>2.5</b>	<b>Previous Study</b>	<b>16</b>
<b>2.5.1</b>	<b>Previous study on numerical simulations of MASnI<sub>3</sub> as an absorber layer</b>	<b>16</b>
<b>2.5.2</b>	<b>Previous study on fabrication of MASnI<sub>3</sub> as an absorber layer</b>	<b>23</b>
<b>CHAPTER 3: METHODOLOGY</b>		<b>27</b>
<b>3.1</b>	<b>Overview</b>	<b>28</b>
<b>3.2</b>	<b>Flowchart</b>	<b>28</b>
<b>3.3</b>	<b>Simulation Analysis</b>	<b>30</b>

3.3.1	SCAPS-1D Software	30
3.3.2	SCAPS-1D simulation for MASnI <sub>3</sub> on PSC	32
3.3.3	Method of Analysis	37
<b>CHAPTER 4: RESULTS AND DISCUSSION</b>		<b>39</b>
4.1	Analysis of MASnI <sub>3</sub> and TiO <sub>2</sub> (ETL)	40
4.1.1	Analysis of working temperature I	40
4.1.2	Analysis of the variation of MASnI <sub>3</sub> thickness I	42
4.1.3	Analysis of the variation of Doping donor density I	45
4.1.4	Analysis of the variation of Doping acceptor density I	48
4.1.5	Analysis of the variation of Defect density at the interface I	51
4.2	Analysis of MASnI <sub>3</sub> and SnO <sub>2</sub> (ETL)	54
4.2.1	Analysis of working temperature II	54
4.2.2	Analysis of the variation of MASnI <sub>3</sub> thickness II	57
4.2.3	Analysis of the variation of Doping donor density II	60
4.2.4	Analysis of the variation of Doping acceptor density II	62
4.2.5	Analysis of the variation of Defect density at the interface II	64
4.3	Analysis of efficiency based on optimum value for all parameters.	66
4.3.1	Analysis of the efficiency based on the optimization value for MASnI <sub>3</sub> as an absorber and TiO <sub>2</sub> as an ETL.	66

4.3.2	Analysis of the efficiency based on the optimization value for MASnI3 as an absorber and SnO2 as an ETL.	69
<b>CHAPTER 5: CONCLUSION AND FUTURE WORKS</b>		<b>72</b>
5.1	Conclusion	73
5.2	Future Work	74
<b>REFERENCES</b>		<b>75</b>



## LIST OF FIGURES

Figure 2.1: Renewable energy net capacity additions by technology from 2015 to 2027 [3].	7
Figure 2.2: Monocrystalline solar cells [5].	9
Figure 2.3: Cadmium Telluride [6].	10
Figure 2.4: Perovskite Solar cell [8].	11
Figure 2.5: PSC sandwiched structure.	11
Figure 2.6: Working principle of PSC.	12
Figure 2.7: Diagram of spectral irradiation under AM1.5 [12].	13
Figure 2.8: Solar cell I-V characteristic curve ( $V_{oc}$ ).	14
Figure 2.9: Solar cell I-V characteristic curve ( $J_{sc}$ ).	15
Figure 3.1: Flowchart for this project.	28
Figure 3.2: The action panel of SCAPS-1D.	31
Figure 3.3: Cell definition panel for solar cell's structure in SCAPS-1D.	32
Figure 3.4: Simulated PSC structure ( $MA_{sn}I_3$ ) with $TiO_2$ (ETL).	33
Figure 3.5: PSC Solar cell structure with $TiO_2$ (ETL).	33
Figure 3.6: Simulated PSC structure ( $MA_{sn}I_3$ ) with $SnO_2$ (ETL).	34
Figure 3.7: PSC Solar cell structure with $SnO_2$ (ETL).	34

Figure 4.1: The analysis of efficiency based on the variation of working temperature using TiO <sub>2</sub> . .....	41
Figure 4.2: The analysis of efficiency based on the variation of absorber thickness using TiO <sub>2</sub> . .....	44
Figure 4.3: The analysis of efficiency based on the variation of doping donor density using TiO <sub>2</sub> . .....	46
Figure 4.4: The analysis of efficiency based on the variation of doping acceptor density using TiO <sub>2</sub> . .....	49
Figure 4.5: Analysis for the variation of defect density at MASnI <sub>3</sub> /TiO <sub>2</sub> . .....	52
Figure 4.6: The analysis of efficiency based on the variation of working temperature using SnO <sub>2</sub> . .....	55
Figure 4.7: The analysis of efficiency based on the variation of absorber thickness using SnO <sub>2</sub> . .....	58
Figure 4.8: The analysis of efficiency based on the variation of doping donor density using SnO <sub>2</sub> . .....	61
Figure 4.9: The analysis of efficiency based on the variation of doping acceptor density using SnO <sub>2</sub> . .....	63
Figure 4.10: Analysis of the variation of defect density at MASnI <sub>3</sub> /SnO <sub>2</sub> . .....	65
Figure 4.11: J-V curve for the optimized PSC structure using TiO <sub>2</sub> as an ETL. ....	68
Figure 4.12: J-V curve for the optimized PSC structure using SnO <sub>2</sub> as an ETL. ....	70

## LIST OF TABLES

Table 2.1: Output parameters for different types of structures by simulation method. .....	22
Table 2.2: Output parameters for different types of structures by fabrication method. .....	26
Table 3.1 Input parameters of numerical analyzing the PSC using TiO <sub>2</sub> (ETL).....	35
Table 3.2: Input parameters of numerical analyzing the PSC using SnO <sub>2</sub> (ETL).....	36
Table 4.1: Constant parameter value for working temperature analysis using TiO <sub>2</sub> .	40
Table 4.2: The analysis of efficiency based on the variation of working temperature using TiO <sub>2</sub> . .....	41
Table 4.3: The constant set parameter value for Absorber thickness analysis using TiO <sub>2</sub> . .....	43
Table 4.4: The analysis of efficiency based on the variation of absorber thickness using TiO <sub>2</sub> . .....	43
Table 4.5: The constant set parameters value for doping donor analysis using TiO <sub>2</sub> . .....	46
Table 4.6: Analysis of efficiency based on the variation of doping donor density using TiO <sub>2</sub> . .....	46
Table 4.7: The constant set parameter value for doping acceptor analysis using TiO <sub>2</sub> . .....	48
Table 4.8: Analysis of efficiency based on the variation of doping acceptor density using TiO <sub>2</sub> . .....	49



Table 4.9: The constant set parameter value for defect density analysis using TiO <sub>2</sub> . .....	51
Table 4.10: Analysis of efficiency based on the variation of defect density at MASnI <sub>3</sub> /TiO <sub>2</sub> . .....	52
Table 4.11: Constant parameter value for working temperature analysis using SnO <sub>2</sub> . .....	55
Table 4.12: The analysis of efficiency based on the variation of working temperature using SnO <sub>2</sub> . .....	56
Table 4.13: The constant set parameter value for absorber thickness analysis using SnO <sub>2</sub> . .....	57
Table 4.14: The analysis of efficiency based on the variation of absorber thickness using SnO <sub>2</sub> . .....	58
Table 4.15: The constant set parameters value for doping donor analysis using SnO <sub>2</sub> . .....	60
Table 4.16: Analysis of efficiency based on the variation of doping donor density using SnO <sub>2</sub> . .....	60
Table 4.17: The constant set parameter value for doping acceptor analysis using SnO <sub>2</sub> . .....	62
Table 4.18: Analysis of efficiency based on the variation of doping acceptor density using SnO <sub>2</sub> . .....	63
Table 4.19: The constant set parameter value for defect density analysis using SnO <sub>2</sub> . .....	65
Table 4.20: Analysis of efficiency based on the variation of defect density at MASnI <sub>3</sub> /SnO <sub>2</sub> . .....	65
Table 4.21: The optimized value for all parameters with TiO <sub>2</sub> as an ETL. ....	67
Table 4.22: The optimized value for all parameters with SnO <sub>2</sub> as an ETL.....	69

## LIST OF SYMBOLS AND ABBREVIATIONS

SCAPS	:	Solar Cell Capacitance Simulator
PV	:	Photovoltaic
PCE	:	Power Conversion Efficiency
ETL	:	Electron Transport Layer
HTL	:	Hole Transport Layer
ETM	:	Electron Transport Materials
HTM	:	Hole Transport Materials
PSC	:	Perovskite Solar Cells
MASnI <sub>3</sub>	:	Methylammonium Tin Triiodide
TiO <sub>2</sub>	:	Titanium dioxide
SnO <sub>2</sub>	:	Tin dioxide
SDGs	:	Sustainable Development Goals
c-Si	:	Crystalline Silicon
DSSC	:	Dye-Sensitized Solar Cells
CH <sub>3</sub> NH <sub>3</sub> PbI <sub>3</sub>	:	Methylammonium lead iodide
TCO	:	Transparent Conductive Oxide
FTO	:	Fluorotin Oxide
ITO	:	Indium Tin Oxide

Voc	:	Voltage Open Circuit
Jsc	:	Current Short Circuit
FF	:	Fill Factor
WO <sub>3</sub>	:	Tungsten Trioxide
PEDOT:PSS	:	Poly(3,4-ethylenedioxythiophene) Polystyrene Sulfonate
FASnI <sub>3</sub>	:	Formamidinium Tin Iodide
CH <sub>3</sub> NH <sub>3</sub> SnI <sub>3</sub>	:	Methylammonium Tin Iodide
Sn-Ge	:	Tin-Germanium
I-V	:	Current-Voltage
Cu <sub>2</sub> O	:	Copper(I) Oxide
eV	:	Electrovolt



## CHAPTER 1:

### INTRODUCTION



#### 1.1 Background

The rapid progress of solar energy technologies has driven the search for efficient and environmentally friendly photovoltaic materials. Among the various candidates, perovskite solar cells (PSC) have shown promise due to their exceptional power conversion efficiency (PCE) and low-cost manufacturing processes. However, the incorporation of lead-based perovskite materials into PSC has raised concerns about their toxicity and long-term stability. To address these challenges and pave the way for sustainable photovoltaics, researchers have turned their attention to developing lead-free perovskite solar cells. By replacing lead with alternative materials, it offers the potential for highly efficient solar cells with a lower environmental impact. The aim of this paper is to provide an overview of the current status of lead-free perovskite

solar cells and examine their unique properties and performance characteristics. Key research efforts to optimize the structure and composition of lead-free perovskite materials and their impact on device performance, stability, and scalability are discussed. The successful development of lead-free perovskite solar cells is promising for the future of renewable energy. By combining highly efficient conversion of sunlight into electricity with a lower environmental impact, these next-generation solar cells have the potential to revolutionize the photovoltaic industry and contribute to a more sustainable and greener future. Overall, this paper aims to provide a comprehensive overview of MASnI<sub>3</sub>-based lead-free perovskite solar cells and highlight their importance, current advances, and future prospects in the pursuit of sustainable photovoltaics.

## 1.2 Problem Statement

Perovskite materials are relatively simple and inexpensive to produce, making them an attractive option for large-scale solar energy deployment. Additionally, perovskite materials can be used in flexible and lightweight solar cells, which could open up new applications for solar energy in areas such as wearable electronics, building-integrated photovoltaics, and wearable devices. However, toxicity and instability are two major problems associated with the use of lead-containing perovskite materials in solar cells. Improper handling and disposal of lead can pose a risk to the environment, while degradation of lead-based perovskite materials due to exposure to environmental factors can affect their reliability and long-term stability. Therefore, this project aims to develop a lead-free perovskite solar cell using SCAPS software, optimize the parameters and achieve a high-power conversion efficiency (PCE) of  $\geq 25\%$  based on the Best Research-Cell Efficiency Chart [1].

### 1.3 Project Objectives

This project has two objectives which are:

1. To simulate a lead-free perovskite solar cell utilizing MASnI<sub>3</sub> as perovskite using SCAPS software.
2. To determine the effect of MASnI<sub>3</sub> as an absorber layer in perovskite solar cell with TiO<sub>2</sub> and SnO<sub>2</sub> as an ETL layer.

### 1.4 Project Scope

The focus of this research project is on the design and optimization of a MASnI<sub>3</sub> perovskite solar cell. The aim is to simulate the behavior of the electron transport layer with two different materials (TiO<sub>2</sub> and SnO<sub>2</sub>), analyze the performance of the solar cell and determine the best material combination for improved efficiency and stability. The project uses SCAPS simulation software to evaluate the behavior of the solar cell under various conditions. The aim is to determine the optimal configuration of the electron transport layers in terms of power conversion efficiency and long-term stability by analyzing the simulation results. This research contributes to the development of lead-free perovskite solar cells and advances the field of renewable energy.

### 1.5 Importance of Study

The development of lead-free perovskite solar cells using the SCAPS software represents a significant step towards sustainable and environmentally friendly practices in line with the United Nations Sustainable Development Goals (SDGs). This research not only aims to improve the efficiency and not only does it improve the stability of perovskite solar cells (PSCs), but also contributes to the further development of technologies that support important SDGs. By using SCAPS software,

researchers can optimize the performance of PSCs, improving their efficiency and stability. This optimization process is in direct line with SDG 7 (Affordable and Clean Energy), which highlights the importance of promoting renewable energy sources for widespread access to affordable and sustainable energy. Lead-free perovskite solar cells have the potential to significantly contribute to clean energy production, reducing dependence on fossil fuels and mitigating environmental impacts. Additionally, the introduction of lead-free perovskite materials in PSCs supports SDG 12 (Responsible Consumption and Production).

Lead is a toxic substance that poses a threat to human health and the environment. By eliminating lead from the production process, this research minimizes the environmental hazards associated with the disposal of lead-containing PSCs and promotes responsible consumption and sustainable production practices. In addition, the development of lead-free perovskite solar cells using SCAPS software is in line with SDG 9 (Industry, Innovation, and Infrastructure). It promotes advances in renewable energy technologies and contributes to the innovation and infrastructure needed for a sustainable future. By pushing the boundaries of perovskite solar cell efficiency and stability, this research paves the way for integrating these technologies into existing infrastructure and facilitating the transition to cleaner and more sustainable energy systems.

## **1.6 Thesis Outline**

The investigation of lead-free perovskite  $\text{MASnI}_3$  solar cells using SCAPS simulation was presented about the recurrent difficulties and the inventive structure or improvement of the system. All findings related to this task have been described in each part of this report as follows.

**Chapter 1:** This section serves as an introductory presentation and provides an overview of the study of MASnI<sub>3</sub>-based lead-free perovskite solar cells. It will address the problem statement, objectives, scope, significance and outline to provide a clear understanding of the study and project.

**Chapter 2:** In this section, an examination of relevant literature sources related to the project is carried out. Extensive research has been carried out in the past, providing valuable insights and enabling a comprehensive understanding of the project context.

**Chapter 3:** This section examines the steps to complete the project. To design the solar cell using SCAPS simulation, a few steps need to be completed. Project flow diagram, block diagram, the technique used, and explanations of the manipulated parameters are given.

**Chapter 4:** This section presents the results of the semester and highlights the achievements achieved. Project results based on simulation testing and project completion are also discussed.

**Chapter 5:** This section presents conclusions and recommendations for studying lead-free perovskite MASnI<sub>3</sub> solar cells using SCAPS simulation. This section also includes a project overview, project discovery, and other suggestions for improving the project.



## CHAPTER 2:

### BACKGROUND STUDY



This part will talk about sources or articles that identified with the project. Some sources and specialists previously did, and insights regarding this project are known from it to understand better about the project. In this section, the theoretical foundation, literature review of previous work, and the outlines about the past work will be secured.

## 2.1 Photovoltaic (PV)

Solar energy stands out as a sustainable, renewable and self-sufficient energy source, distinguishing it from finite options such as fossil fuels. The use of solar radiation to generate electricity through human-invented solar technologies represents a crucial aspect of this energy paradigm. Among these technologies, photovoltaic solar panels are proving to be a widely used method of generating solar energy. These modules are based on the principle of the photovoltaic effect and can convert sunlight into usable electricity. This conversion occurs when photons from the sun excite electrons in the semiconductor of a PN junction, resulting in the generation of an electric current. The use of photovoltaic systems is particularly important given the enormous potential of solar radiation, which is around ten thousand times greater than global electrical energy consumption. While the first conventional photovoltaic technologies were patented in the late 1950s, their use initially focused on powering orbiting satellites [2]. However, in recent years, solar photovoltaics has made remarkable progress, cementing its status as a significant and evolving sustainable energy source.

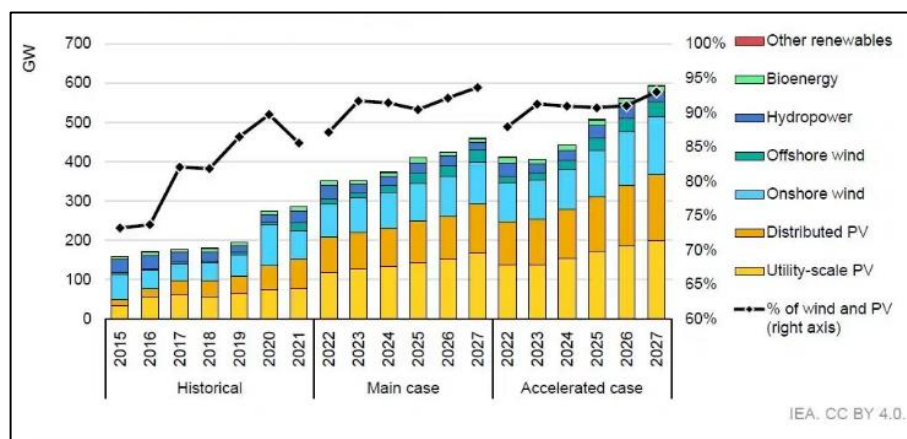


Figure 2.1: Renewable energy net capacity additions by technology from 2015 to 2027 [3].

Figure 2.1 shows net renewable energy capacity increases by technology from 2015 to 2027 [3]. The increase in solar energy capacity could exceed 234 GW. Despite the stability of solar energy, the ongoing Covid-19 crisis presents new challenges for renewable energy. These challenges include financial constraints, shifts in government spending priorities and uncertainties surrounding electricity consumption. Nevertheless, the basic principles of the expansion of renewable energies remain unchanged [3].

## 2.2 Generation of Solar Cell

In the early stages of solar cell development, the predominant materials were crystalline silicon (c-Si) or germanium, doped within a PN junction, with phosphorus and boron. While crystalline silicon solar cells have commendable power conversion efficiency, the manufacturing process is characterized by high costs due to the use of complicated equipment. Silicon solar cells, made primarily of crystalline silicon, are considered the most efficient photovoltaic devices within a single cell. These cells are particularly suitable for photovoltaic applications with an energy band gap of 1.1 eV [4]. It is noteworthy that the solar cells of this generation are made from thin silicon wafers, which gives them the name monocrystalline solar cells because they are made from large single crystals [5].

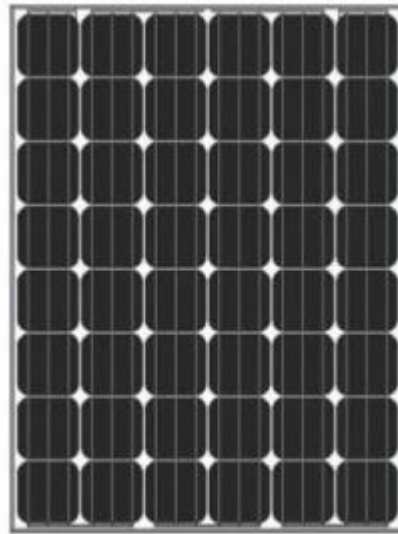


Figure 2.2: Monocrystalline solar cells [5].

The second generation of solar cells, called thin-film solar cells, is characterized by its thinness, which is only a few micrometers in contrast to the thicker silicon-based crystalline cells [6]. In theory, these thin film solar cells have the potential to provide lower cost electricity compared to their crystalline silicon counterparts. These solar cells consist of successive thin layers and are deposited on a wide and inexpensive substrate such as glass, polymer or metal. This design allows for flexibility and low weight, allowing thin films to be incorporated into versatile and easily integrated structures, particularly building components.

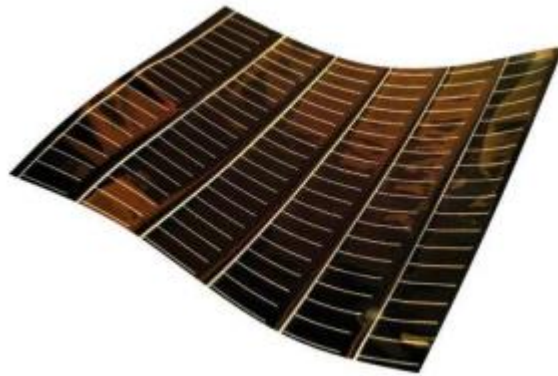


Figure 2.3: Cadmium Telluride [6].

The emergence of third-generation photovoltaic cells is due to the high costs associated with first-generation solar cells, concerns about toxicity, and limitations in material availability for second-generation solar cells. Third generation solar cells differ significantly from their predecessors and do not rely on the architecture of other PN junctions. This new generation includes a variety of materials, including nanomaterials, silicon wires, solar inks using conventional printing press technologies, organic materials, dyes, and conductive plastics [7]. A notable example is dye-sensitized solar cells (DSSC), which offer improved efficiency in a wider range of solar energy, cost-effectiveness and non-toxicity, making them accessible to a wider user base with diverse applications [8]. In addition, DSSC is characterized by high efficiency, cost-effectiveness, simple manufacturing processes, environmental friendliness, transparency and adaptability.

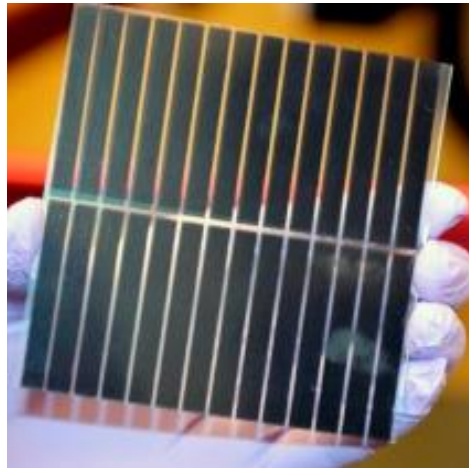


Figure 2.4: Perovskite Solar cell [8].

### 2.3 Perovskite Solar cell

The main component in PSC is a composed semiconductor, absorber ( $\text{CH}_3\text{NH}_3\text{PbI}_3$ ), and HTL that is sandwiched together in between the transparent conductive oxide (TCO) [9]. It is critical to optimize each of them to increase overall efficiency. Figure 2.5 depicts the sandwiched structure of PSC.



Figure 2.5: PSC sandwiched structure.

The discovery of perovskite in 2009 marked a significant breakthrough in solar cell technology, earning it classification as a third generation of solar cells. Perovskite solar cells (PSCs) are characterized by three fundamental layers: the electron transport

layer (ETL), which utilizes  $\text{TiO}_2/\text{SnO}_2$ , the Hole Transport Layer (HTL), which uses  $\text{Cu}_2\text{O}$ , and the absorber layer contains perovskite. These layers are arranged in a complicated manner and form a solar panel [10]. The workflow begins with light penetrating the surface structure and reaching the perovskite layer, where energy absorption leads to the formation of electron-hole pairs. Conceptualizing the perovskite region as an intrinsic region creates a PN junction that triggers the migration of electrons and holes in opposite directions influenced by the built-in electric field in both HTL and ETL. Electrons and holes then reach the respective electrodes on both sides, enter the external circuit and generate a photocurrent [11]. The electrons end their journey in the conductive electrode or transparent conductive oxide (TCO). Commonly used TCOs include fluorotin oxide (FTO) and indium tin oxide (ITO). These TCOs provide a crucial path for electrons to reach the load, be it a light bulb or a battery. To visually illustrate this complicated process, Figure 2.6 shows the working principle of PSC.

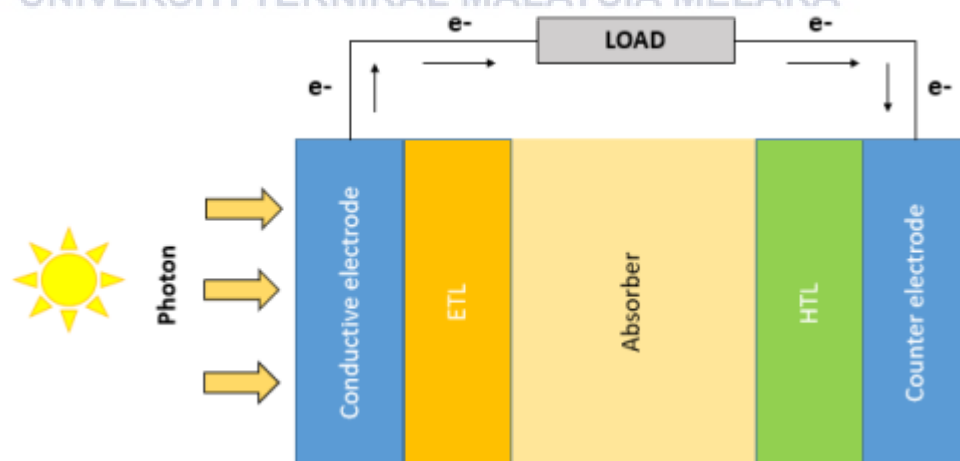


Figure 2.6: Working principle of PSC.

Figure 2.7 shows how the spectral irradiance of light changes as its wavelength changes. The substance we use in the light absorbing layer should work well at high spectrum light irradiation wavelengths [12].

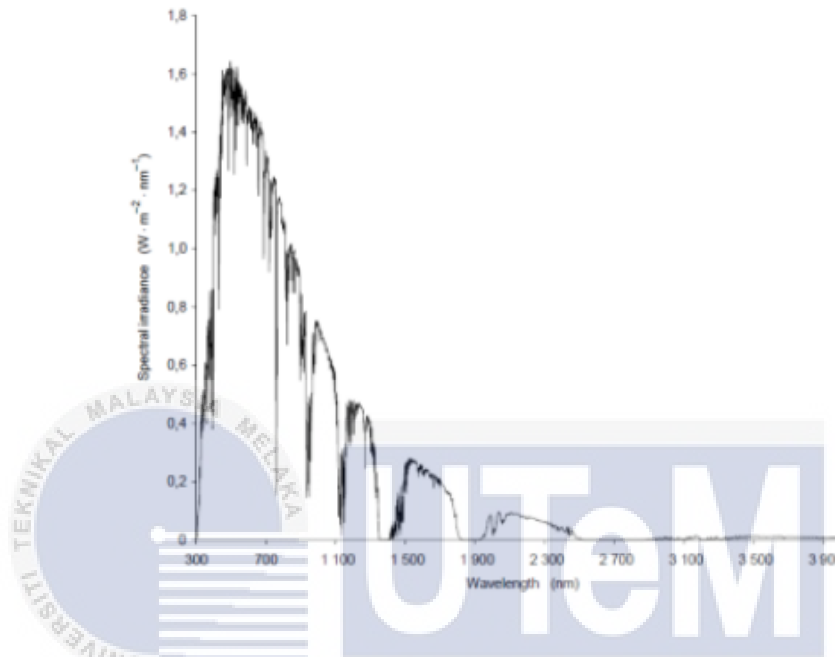


Figure 2.7: Diagram of spectral irradiance under AM1.5 [12].

## 2.4 Key Parameter of Solar Cell's interest

### 2.4.1 Voltage Open Circuit (Voc)

Voltage open circuit ( $V_{oc}$ ) is a crucial parameter that indicates the voltage across a circuit when it is open. Essentially, it refers to the potential difference in a circuit under conditions where no current is flowing. The relationship between current flow and open circuit voltage is inversely proportional - as current flow through the circuit decreases, open circuit voltage tends to increase. The maximum voltage is reached when the circuit is fully open, which is characterized by a significantly high resistance and complete absence of current flow. For a more detailed visual representation, Figure 2.8 provides a clear representation of the complex dynamics associated with voltage open circuit ( $V_{oc}$ ) [13].



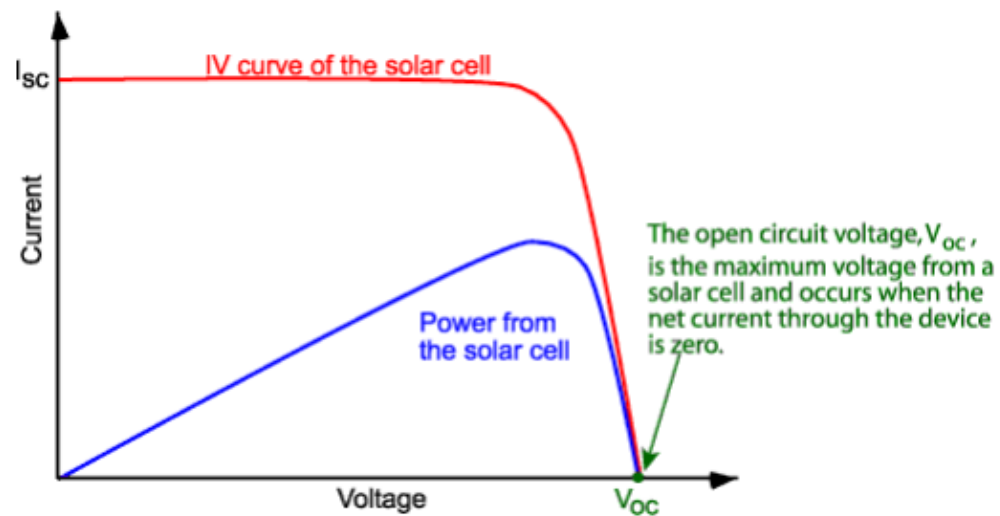


Figure 2.8: Solar cell I-V characteristic curve ( $V_{oc}$ ).

#### 2.4.2 Current Short Circuit ( $J_{sc}$ )

Current short-circuit ( $J_{sc}$ ) is a fundamental parameter that characterizes the current that flows through the external circuit of a solar cell when the voltage across the cell is reduced to zero, effectively short-circuiting the system. This current, measured in amperes, is denoted by the abbreviation  $J_{sc}$ . The short-circuit current is closely linked to the photon flux incident on the solar cell, which in turn is influenced by the wavelength of the incident light. Figure 2.9 provides a detailed representation of the dynamics of short-circuit current, visually depicting its relationship to incident light and emphasizing its importance in understanding the behavior of solar cells [13].

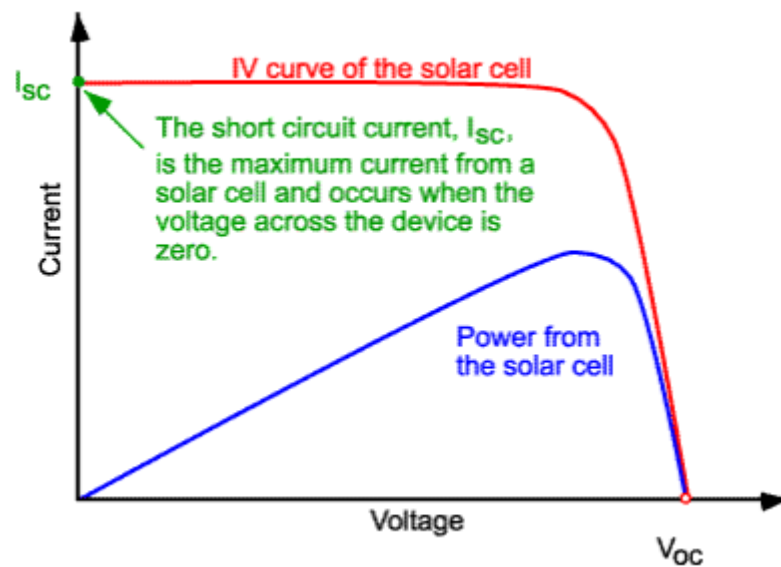


Figure 2.9: Solar cell I-V characteristic curve ( $I_{sc}$ ).

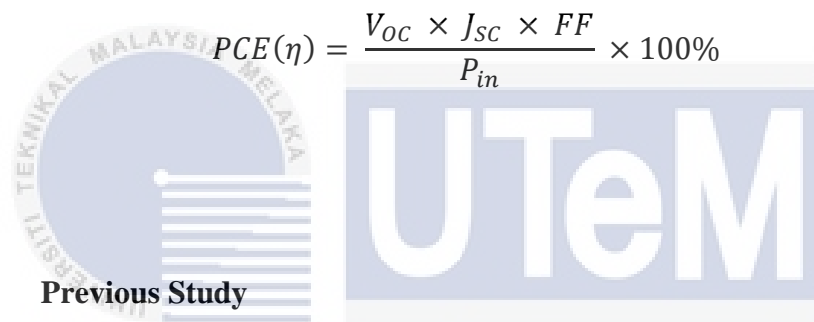
### 2.4.3 Fill Factor (FF)

The fill factor, commonly abbreviated as FF, serves as a crucial measurement when assessing the efficiency of a solar cell and represents the maximum achievable power output of the cell. This factor is defined as the ratio of the maximum power generated to the product of short-circuit current ( $I_{sc}$ ) and open-circuit voltage ( $V_{oc}$ ). A higher fill factor corresponds to improved solar cell efficiency. Fill factor improvement includes optimizing shunt resistance, reducing series resistance, and minimizing diffusion and charge transfer overvoltage. Achieving an optimal fill factor is crucial for maximizing the overall efficiency of a solar cell [14]. The mathematical expression for FF is as follow [13]:

$$FF = \frac{I_{mpp}V_{mpp}}{I_{sc}V_{sc}}$$

#### 2.4.4 Power Conversion Efficiency (PCE)

Power Conversion Efficiency (PCE) is a critical measure of a solar cell's effectiveness in converting incident light output into electrical energy. This efficiency is crucial for how much energy can be generated from a certain amount of sunlight. A higher PCE means a solar cell can produce more energy. PCE is a key parameter that influences the overall performance and utility of solar cells. When calculating PCE, it is about the ratio of the incident light output to the electrical power generated. PCE can be calculated using the mathematical expression [13] as follows:

$$PCE(\eta) = \frac{V_{oc} \times J_{sc} \times FF}{P_{in}} \times 100\%$$


#### 2.5 Previous Study

##### 2.5.1 Previous study on numerical simulations of MASnI3 as an absorber layer

In a 2021 paper published in *Optical Materials*, H. Alipour and A. Ghadimi focus on optimizing lead-free perovskite solar cells (PSCs) in a normal structure while addressing concerns about lead toxicity. The study presents a novel approach by integrating WO<sub>3</sub> and an anhydrous PEDOT:PSS composite as a hole transport layer into the PSC architecture, providing a more environmentally friendly alternative [15]. Using SCAPS-1D simulation, the authors conduct a comprehensive analysis of the electrical and optical properties of the lead-free PSC under various conditions. This simulation plays a critical role in predicting and optimizing device performance and provides valuable insight into the effects of material composition on efficiency and stability. The research published in *Optical Materials* contributes to the broader

scientific discourse on lead-free PSC technology and demonstrates its relevance within the optical and materials science community. The study's focus on innovative materials and simulation techniques underscores its importance in advancing the field toward more efficient and sustainable perovskite solar cells.

The research conducted by M. Vishnuwaran, K. Ramachandran, P. Roy and A. Khare is presented in their paper “SCAPS simulated FASNI3 and MASNI3 based PSC solar cells: A comparison of device performance” published in IOP The Materials Science in 2022 examines the comparative performance of perovskite solar cells (PSCs) that use FASNI3 and MASNI3 as active materials. Using SCAPS simulation, the authors investigate the electronic and optical properties of these perovskite materials with the aim of determining their impact on the overall device efficiency. This recent and relevant study provides valuable insights into the structural and electronic properties of FASNI3 and MASNI3 and highlights their respective roles in influencing PSC performance [16]. The use of SCAPS simulation enables comprehensive analysis of electrical and optical parameters under various conditions, thus facilitating predictions of device behavior. The research, published as part of a prestigious conference series, highlights its importance to materials science and engineering, advancing the understanding of perovskite solar cell technology and potentially informing future device design and optimization efforts.

The research conducted by A. K. Al-Mousoi and colleagues, presented in their 2022 paper entitled "Simulation and analysis of lead-free perovskite solar cells with cerium oxide as an electron transport layer" published in RSC Advances, investigates the incorporation of ceria as an electron transport layer in lead-free perovskite solar cells. Solar cells (PSCs). The study addresses growing concerns about the environmental

impact of lead-based PSCs by examining lead-free alternatives. Using simulation techniques and analysis, the authors investigate the performance of PSCs with ceria as an electron transport layer. Particularly noteworthy is the choice of cerium oxide, as it has shown promise for improving the electronic properties of perovskite solar cells [17]. The study represents a significant step in advancing the understanding and development of lead-free perovskite solar cells, with potential implications for sustainable and scalable photovoltaic technologies.

The article entitled “Modeling and numerical simulation of a highly efficient perovskite solar cell with three active layers” authored by H. Abedini-Ahangarkola, S. Soleimani-Amiri and S. Gholami Rudi presents a novel and innovative study in the field of perovskite solar cells (PSCs). The recently published study addresses the search for improved efficiency in PSCs by introducing a unique design with three active layers. The modeling and numerical simulations performed in this research provide valuable insights into the potential improvements achievable through the unconventional multilayer architecture. By departing from the traditional double-layer structures, the authors aim to optimize light absorption and the generation of electron-hole pairs, essential factors for achieving high PSC efficiency [18]. The study contributes to the evolving landscape of PSC research by providing a detailed analysis of the three active layer configurations and illuminating its impact on solar cell performance.

The paper, authored by K. Deepthi Jayan and V. Sebastian, titled “Comprehensive device modeling and performance analysis of MASnI<sub>3</sub>-based perovskite solar cells with diverse ETM, HTM, and back metal contacts,” published in Solar Energy in 2021, provides: a Thorough study of the performance and modeling of perovskite solar

cells (PSCs) based on MASnI<sub>3</sub>. The study focuses on the comprehensive investigation of various elements in the PSC architecture, including the electron transport material (ETM), hole transport material (HTM), and back metal contacts. Through a holistic approach, the authors aim to gain a nuanced understanding of how these components impact the overall efficiency and performance of MASnI<sub>3</sub>-based PSCs. The results provide valuable insights into the intricacies of MASnI<sub>3</sub>-based PSCs and shed light on the nuanced interactions between different materials within the device [19]. The study not only addresses the current knowledge gaps, but also serves as a valuable resource for researchers and practitioners seeking to optimize the performance of MASnI<sub>3</sub>-based perovskite solar cells.

The paper, authored by A. K. Singh, S. Srivastava, A. Mahapatra, J. K. Baral and B. Pradhan, is titled “Performance optimization of lead-free MASnI<sub>3</sub>-based solar cells with 27% efficiency through numerical simulation” and was published in *Optical Materials* in 2021. This work represents a significant contribution to the field of perovskite solar cells (PSCs). The study focuses on the optimization of lead-free MASnI<sub>3</sub>-based solar cells through rigorous numerical simulations and achieves an impressive efficiency of 27%. The pursuit of lead-free alternatives addresses the environmental concerns associated with traditional perovskite materials. The authors use advanced numerical simulation techniques to systematically optimize the device parameters, resulting in a remarkable increase in efficiency. The article was published in *Optical Materials*, a renowned journal in the field, and demonstrates the importance of these findings for the optical and materials science community. The reported efficiency of 27% is a remarkable achievement and highlights the potential of MASnI<sub>3</sub> as a promising candidate for high-performance, environmentally friendly perovskite solar cells [20].

This research not only contributes to the understanding of lead-free PSCs, but also provides valuable insights for ongoing efforts to optimize perovskite solar cell technology for greater efficiency and sustainability.

Authored by A. Hima and published in the International Journal of Energetica in 2020, the paper titled “Enhancing CH<sub>3</sub>NH<sub>3</sub>SNi<sub>3</sub> based solar cell efficient by ETL Engineering” focuses on improving the efficiency of solar cells based on CH<sub>3</sub>NH<sub>3</sub>SNi<sub>3</sub>, a notable member of the perovskite family. The study focuses on the development of the electron transport layer (ETL) as a strategic approach to increase the overall performance of the solar cell [21]. Through the systematic development of ETL, the author aims to improve charge transport and charge collection, which are crucial influencing factors on the efficiency of perovskite solar cells. The paper, published in the International Journal of Energetica, contributes to the field of energy research by exploring new ways to increase the efficiency of CH<sub>3</sub>NH<sub>3</sub>SNi<sub>3</sub>-based solar cells. Despite the conciseness of the paper, it highlights the importance of ETL technology as a viable strategy to advance perovskite solar cell technology. This research adds to the ongoing discourse on improving the efficiency of perovskite solar cells and provides insights that could inform future developments in the search for more efficient and sustainable photovoltaic devices.

The paper entitled “Numerical simulation of a high efficiency lead-free all-perovskite tandem solar cell” authored by N. Singh, A. Agarwal and M. Agarwal and published in Solar Energy in 2020 represents a significant contribution to the field solar cell technology with a particular focus on lead-free perovskite tandem solar cells. The study uses numerical simulation techniques to investigate and optimize the performance of tandem solar cells. The goal is to achieve high efficiency while

addressing environmental concerns associated with lead-containing perovskite materials [22]. The paper, published in *Solar Energy*, a renowned journal in the field of renewable energy, highlights the importance of numerical simulations for the design and evaluation of advanced solar cell architectures. The reported results contribute to the understanding of lead-free perovskite tandem solar cells and their potential to achieve high efficiency. The use of numerical simulations enables a systematic investigation of various parameters and provides valuable insights into the factors that influence the performance of the tandem solar cell.

The one by T. Minemoto et al. Authored article entitled “Theoretical Analysis of Band Alignment at Back Junction in Sn-Ge Perovskite Solar Cells with Inverted P-i-N Structure”, published in *Solar Energy Materials and Solar Cells* in 2020, delves deeply into the theoretical analysis of band alignment in Sn-Ge perovskite solar cells. The study specifically focuses on devices with an inverted P-i-N structure and uses theoretical models to investigate band alignment at the posterior junction. The choice of Sn-Ge perovskite materials is notable as it deviates from traditional lead-based compositions and takes into account concerns about environmental impact [23]. The article was published in *Solar Energy Materials and Solar Cells*, a renowned journal in the field of solar cell materials and technologies and provides insights into the fundamental aspects of Sn-Ge perovskite solar cells and their potential for improved performance. The use of theoretical analysis enables a detailed study of tape alignment and provides a fundamental understanding of the electronic properties critical to device efficiency.



Based on all the previous study on numerical simulation of MASnI<sub>3</sub> as an absorber layer above, Table 2.1 shows the output obtained for different types of PSC structures.

Table 2.1: Output parameters for different types of structures by simulation method.

Year	Structure	Voc	Jsc	FF	PCE	Ref.
2022	FTO/P3HT/MASnI <sub>3</sub> /PCBM/Au	1.081	34.64	63.36	23.74	[16]
2022	FTO/CeO <sub>x</sub> /MASnI <sub>3</sub> /Spiro- OMeTAD/Au	0.92	30.79	62.86	17.77	[17]
2022	FTO/TiO <sub>2</sub> /MASnI <sub>3</sub> / MAPbI <sub>3</sub> /FAMASnGeI <sub>3</sub> /Spiro- OMeTAD/Au	1.2	30.7	83.31	30.77	[18]
2021	FTO/PC61BM/MASnI <sub>3</sub> /PEDOT : PSS + WO <sub>3</sub> /Cu	0.86	23.23	74.94	14.96	[15]
2021	Glass/FTO/PCBM/ MASnI <sub>3</sub> /CuI/Au	1.056	34.27	69.23	25.05	[19]
2021	FTO/TiO <sub>2</sub> /MASnI <sub>3</sub> / Cu <sub>2</sub> O /Au	1.203	25.97	87.79	27.43	[20]
2020	ITO/PC61BM/MASnI <sub>3</sub> /PEDOT : PSS/Ag	0.75	27	62.25	12.58	[21]
2020	FTO/TiO <sub>2</sub> /MAPbI <sub>3</sub> /Spiro- OMeTAD/Au	1.16	24.42	87.73	24.77	[22]
2020	FTO/TiO <sub>2</sub> /MASnI <sub>3</sub> / MAPbI <sub>3</sub> /SpiroOMeTAD/Au	1.15	30.87	85.29	30.29	[23]

### 2.5.2 Previous study on fabrication of $\text{MASnI}_3$ as an absorber layer

The paper, authored by A. Bouich, J. Marí-Guaita, B. M. Soucase, and P. Palacios, entitled “Fabrication of highly efficient and stable lead-free solar cells by antisolvent quenching technique,” published in *Nanomaterials* in 2022, addresses the urgent need for environmentally friendly solar cell technologies and focuses on lead-free alternatives. The study uses antisolvent quenching technique as a strategy to improve the efficiency and stability of lead-free solar cells. The paper, published in *Nanomaterials*, a renowned journal in the field of nanotechnology, highlights the importance of advanced manufacturing techniques for producing high-performance lead-free solar cells [24]. The authors emphasize the importance of antisolvent quenching for optimizing the perovskite film formation process, a crucial factor affecting the overall performance of the solar cells. The use of lead-free materials is consistent with ongoing efforts to mitigate environmental concerns associated with traditional perovskite compositions.

The results from F. Li et al. A study entitled “TRIHYDRAZINE dihydriodide-assisted fabrication of Efficient Formamidinium Tin iodide perovskite solar cell” conducted and published in *Solar RRL* in 2019 examines an innovative approach to producing efficient formamidinium tin iodide ( $\text{FASnI}_3$ ). Perovskite solar cells. The research focuses on the use of trihydrazine dihydriodide as an aid in the manufacturing process with the aim of improving the performance of solar cells. The paper, published in *Solar RRL*, a renowned journal in the field of solar energy research, contributes to the evolving understanding of tin-based perovskite materials as promising candidates for photovoltaic applications. The use of trihydrazine dihydriodide is notable because it introduces a new aspect to the manufacturing process and potentially influences the

morphology and stability of the perovskite film [25]. The reported results provide insights into the mechanisms underlying the improved efficiency of FASnI<sub>3</sub> perovskite solar cells and expand the knowledge base for researchers and practitioners in this field.

The P. Wang et al. with the article entitled “Ion Exchange/Insertion Reactions for Fabrication of Efficient Methylammonium Tin Iodide Perovskite Solar Cells” and published in *Advanced Science* in 2020 examines innovative methods for producing efficient methylammonium tin iodide (MASnI<sub>3</sub>) perovskite solar cells [26]. The research focuses on using ion exchange/insertion reactions as a novel approach to improving the performance of these solar cells. The article, published in *Advanced Science*, a renowned interdisciplinary journal, contributes to the growing body of knowledge about tin-based perovskite materials for solar energy applications. The use of ion exchange and insertion reactions represents a unique strategy in the manufacturing process and potentially influences the composition and properties of the perovskite layer.

The B. P. Nguyen et al. conducted study entitled “Phase formation and local charge transport of lead-free CH<sub>3</sub>NH<sub>3</sub>Sn(I<sub>1-x</sub>Br<sub>x</sub>)<sub>3</sub> (0 ≤ x ≤ 1) perovskite solar cells manufactured by solvent optimization” and published in *Solar Energy* in 2019 presents a thorough investigation of lead-free perovskite solar cells (PSCs). Base of CH<sub>3</sub>NH<sub>3</sub>Sn(I<sub>1-x</sub>Br<sub>x</sub>)<sub>3</sub> composition [27]. The focus of the research is on manipulating solvent properties during the manufacturing process to optimize the performance of the resulting solar cells. The article, published in *Solar Energy*, a renowned journal in the field, addresses the growing interest in lead-free alternatives and examines the effects of solvent optimization on both phase formation and local

charge transport in the perovskite solar cells. The use of the composition  $\text{CH}_3\text{NH}_3\text{Sn}(\text{I}1-x\text{Br}x)_3$  is significant because it is consistent with efforts to develop environmentally friendly and stable perovskite materials.

The research by F. Li et al. entitled “A cation exchange approach to fabricate efficient methylammonium tin iodide perovskite solar cells,” published in the 2019 international edition of *Angewandte Chemie*, investigates a novel method for fabricating efficient methylammonium tin iodide ( $\text{MASnI}_3$ ) perovskite solar cells [28]. The study focuses on a cation exchange approach and presents a unique strategy to improve the performance of perovskite solar cells by manipulating the cation composition. The article, published in the renowned interdisciplinary journal *Angewandte Chemie International Edition*, highlights the importance of innovative manufacturing techniques for the further development of the field of perovskite solar cells.

The Y. Yu et al. A study entitled “Thermal evaporated methylammonium tin triiodide thin films for lead-free perovskite solar cell fabrication” conducted and published in *RSC Advances* in 2016 investigates the fabrication of lead-free perovskite solar cells using thermally evaporated methylammonium tin triiodide ( $\text{MASnI}_3$ ) thin films [29]. The research represents an early contribution to the study of alternative materials and aims to address environmental issues associated with lead-containing perovskite compositions. The article addresses the challenges and opportunities associated with thermally evaporated  $\text{MASnI}_3$  thin films for the fabrication of perovskite solar cells.

Based on all the previous study on fabrication of MASnI<sub>3</sub> as an absorber layer above,

Table 2.2 shows the output obtained for different types of PSC structures.

Table 2.2: Output parameters for different types of structures by fabrication method.

Year	Structure	Voc	Jsc	FF	PCE	Ref.
2022	Spiro-OMeTAD/MASnI <sub>3</sub> / C-TiO <sub>2</sub> /FTO	0.69	32.01	38.09	9.44	[24]
2020	ITO/PEDOT:PSS/MASnI <sub>3</sub> / PC60BM/Ag	0.57	20.68	66	7.78	[25]
2020	ITO/PEDOT:PSS/MASnI <sub>3</sub> / PC61BM/BCP/Ag	0.57	20.68	0.66	7.78	[26]
2019	FTO/c-TiO <sub>2</sub> /m- TiO <sub>2</sub> /MASn(I <sub>0.33</sub> Br <sub>0.67</sub> ) <sub>3</sub> /Spiro- OMeTAD/Au	0.58	11.09	49	3.2	[27]
2019	FTO/c-TiO <sub>2</sub> /m- TiO <sub>2</sub> /MASnI <sub>3</sub> /PTAA/Au	0.486	22.91	64	7.13	[28]
2016	ITO/ PEDOT:PSS/ Poly- TPD/MASnI <sub>3</sub> /C60/BCP/Ag	0.377	12.1	36.6	1.7	[29]

## CHAPTER 3:

### METHODOLOGY



In this section will discuss every process or step which has been taken to complete the project. Besides, the input parameter manipulated in this project are explained in more detail such as working temperature, thickness, defect density and doping density used to perform the project successfully. Furthermore, the processes in designing the  $\text{MASnI}_3$  based lead-free perovskite solar cell are also shown.

### 3.1 Overview

This analysis consists of one part, namely the simulation. The simulation part is carried out using SCAPS-1D software. The PCS structure is studied from various aspects including the working temperature, the thickness of the absorber, the doping density and the defect density. The collected I-V features are used to evaluate the overall performance of the system. The process was repeated using different ETL layer materials (TiO<sub>2</sub> and SnO<sub>2</sub>). Figure 3.1 shows flowcharts for the simulation process.

### 3.2 Flowchart

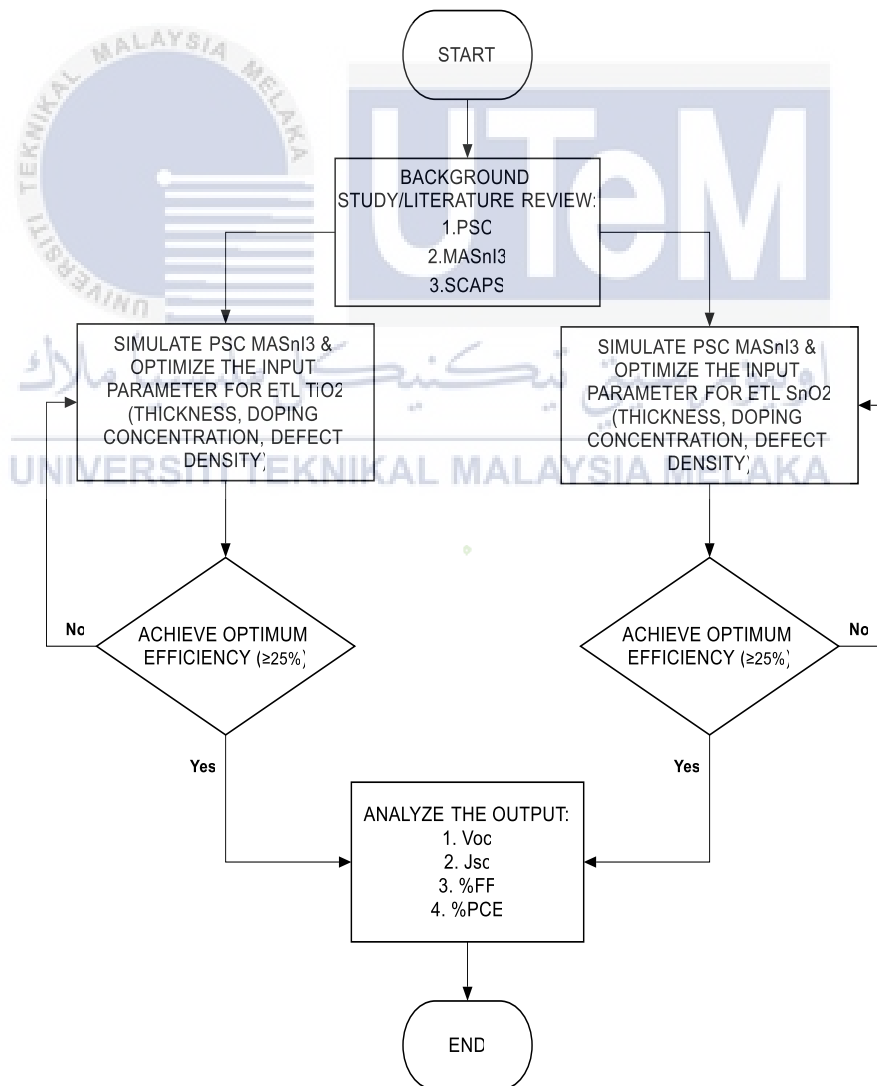


Figure 3.1: Flowchart for this project.

Based on Figure 3.1, this project begins by identifying the research question and objectives. The research question is to investigate the performance of lead-free perovskite solar cells using SCAPS simulation and to optimize the efficiency of the perovskite solar cells. A comprehensive literature review on perovskite solar cells, lead-free perovskite material (MASnI<sub>3</sub>) and SCAPS simulation is carried out. The review is intended to provide a background on the topic and identify the gaps in existing knowledge. Then, the perovskite solar cell is simulated using the SCAPS simulation software with the lead-free perovskite material MASnI<sub>3</sub>, and the input parameters for the electron transport layer SnO<sub>2</sub> and TiO<sub>2</sub> are optimized, including thickness, doping concentration and defect density.

The simulation is then repeated until the best combination of parameters is identified that achieves an optimal efficiency of 25% or more. When the simulation results show that the efficiency of the perovskite solar cell is less than 25%, the output parameters  $V_{oc}$ ,  $J_{sc}$ , %FF and %PCE are analyzed to identify the factors that limit the efficiency. Based on the analysis, the simulation is repeated by adjusting the input parameters until the optimal efficiency is achieved. When the simulation results show that the efficiency of the perovskite solar cell is 25% or more, the output parameters  $V_{oc}$ ,  $J_{sc}$ , %FF and %PCE are analyzed to evaluate the performance of the perovskite solar cell under the optimized conditions. This project will be concluded with a conclusion based on the analysis of the simulation results. The conclusion includes determining the best combination of parameters for the electron transport layer, the performance of the perovskite solar cell in terms of key performance parameters and recommendations for further improvements. This project will contribute to the understanding and optimization of lead-free perovskite solar cells.



### 3.3 Simulation Analysis

#### 3.3.1 SCAPS-1D Software

Achieving accurate predictions of solar cell performance and offering practical assistance in optimizing various geometric and technical factors are critical aspects for successfully performing numerical simulations [10]. At the forefront of this effort is the Solar Cell Capacitance Simulator (SCAPS), an advanced one-dimensional solar cell simulation software carefully developed by dedicated researchers at the Department of Electronics and Information System (ELIS) at Ghent University in Belgium [10][30]. SCAPS stands out for its sophistication, allowing users to delve into the intricacies of solar cell design. With its user-friendly interface, this software allows users to design a p-n junction, seamlessly integrate contacts, and simulate critical properties such as the bandgap energy diagram and the I-V curve of a solar cell.

Its versatility goes beyond the boundaries of a research tool, making it equally accessible for educational purposes and aimed at a wide range of users with different levels of expertise. The diverse features of SCAPS are highlighted in Figure 3.2, where the action panel is depicted and provides a glimpse of the intuitive user interface that makes it easy to set important parameters such as operating point and lighting conditions. This illustration highlights the ease of use of SCAPS, making it beneficial for both novice researchers looking for pedagogical insights and experienced researchers delving into the intricacies of solar energy.

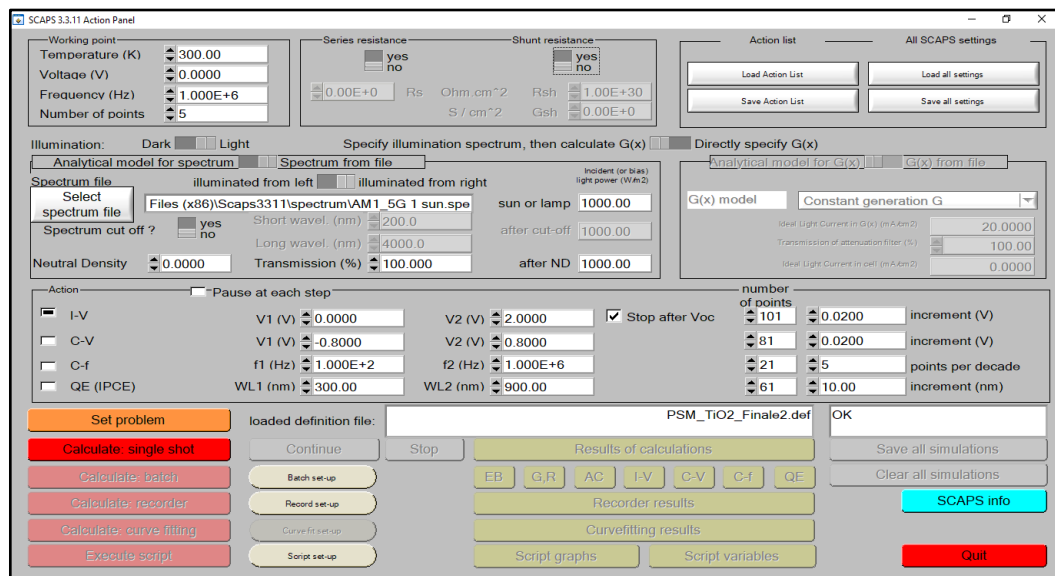


Figure 3.2: The action panel of SCAPS-1D.

Figure 3.3 shows the definition window of the SCAPS software, a central interface that gives users the ability to fine-tune each attribute for individual levels. There are numerous customization options within this panel, allowing users to carefully configure parameters for each layer of the solar panel. It should be noted that the configurations made in this panel are subsequently saved as “.def” files. These files not only encapsulate the intricacies of layer attributes, but also have the flexibility to access and review them using a simple text editor such as Notepad [31].

This dynamic feature not only improves the user experience by allowing granular control over the properties of each file level, but also provides a transparent and accessible way to review and understand the configurations using the generated \'.def\' files. Using a common text editor to view these files, such as: Other tools, such as Notepad, simplify the process even further and ensure that users can easily understand and change solar panel configurations. This integration of user-friendly customization and transparency in file formats highlights the versatility and practicality of SCAPS in facilitating a comprehensive study of solar cell properties.

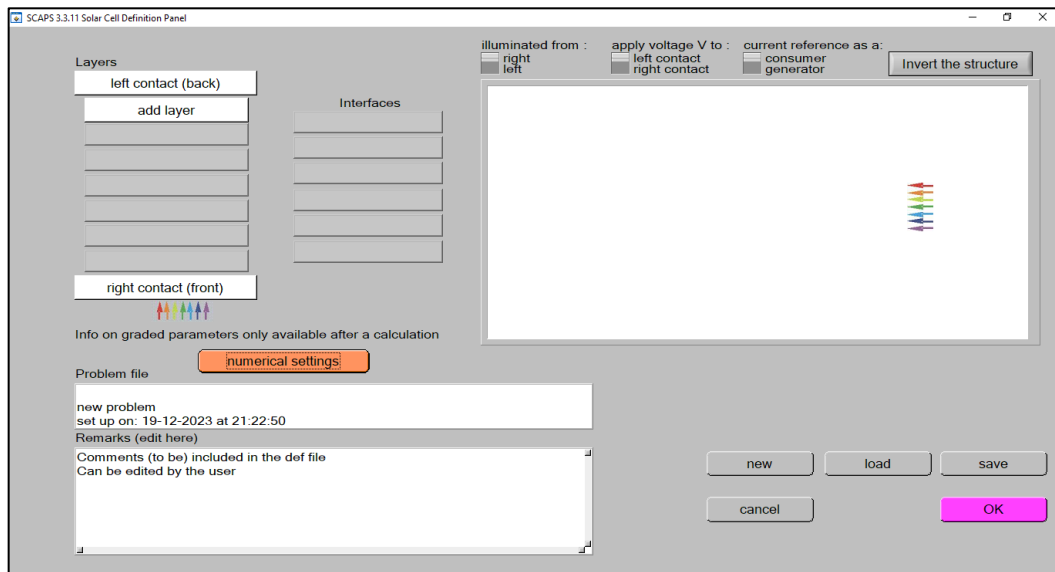


Figure 3.3: Cell definition panel for solar cell's structure in SCAPS-1D.

### 3.3.2 SCAPS-1D simulation for MASnI<sub>3</sub> on PSC

In this research, the modeling framework for the Solid-State Dye-Sensitized Solar Cell (SSDSSC) consists of a sophisticated arrangement of five different layers, each of which plays a crucial role in the functionality of the device. In the first part, the layers consist of fluorine-doped tin oxide (FTO), which serves as a front contact, MASnI<sub>3</sub> as an absorber material and TiO<sub>2</sub> and Cu<sub>2</sub>O, which act as an electron transport layer (ETL) and hole transport layer (HTL), respectively. The ensemble is completed by gold (Au), which serves as a back contact, which is explained in the graphical representations in Figure 3.4 and Figure 3.5.

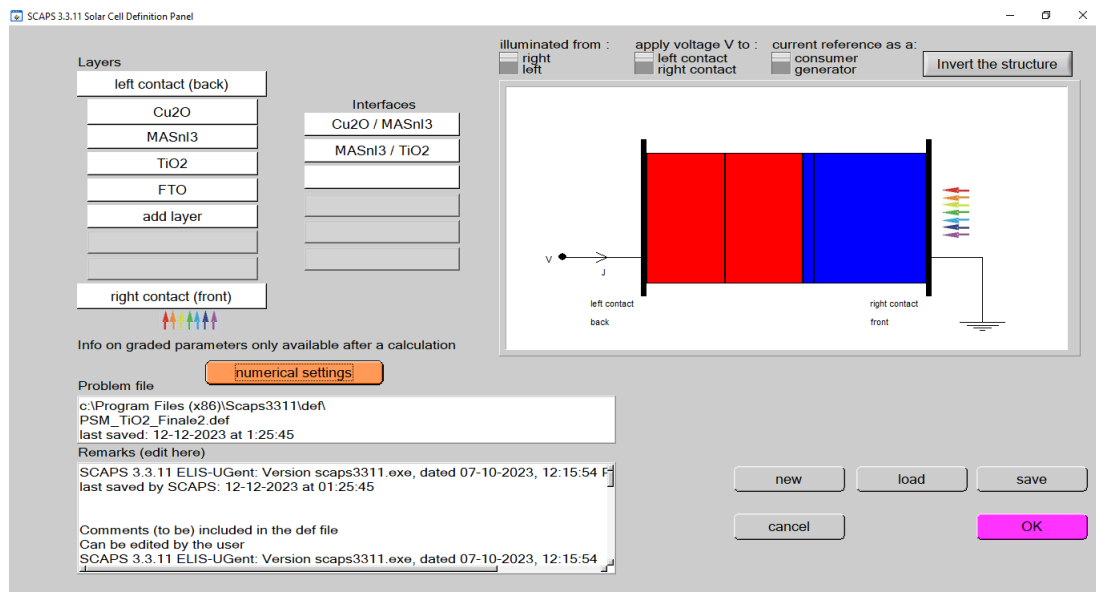


Figure 3.4: Simulated PSC structure (MASnI3) with TiO2 (ETL).

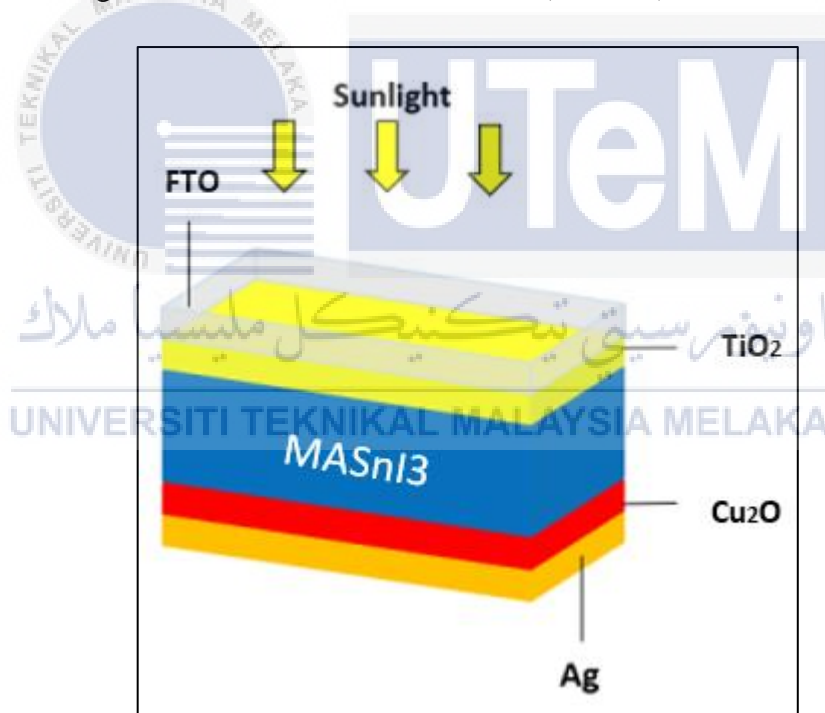


Figure 3.5: PSC Solar cell structure with TiO2 (ETL).

The second part where SnO<sub>2</sub> was used as ETL. The layers consist of fluorine-doped tin oxide (FTO), which serves as a front contact, MASnI<sub>3</sub> as an absorber material, and SnO<sub>2</sub> and Cu<sub>2</sub>O, which act as an electron transport layer (ETL) and hole transport layer (HTL), respectively. The ensemble is rounded off by gold (Au), which

serves as a back contact, which is explained in the graphical representations in Figure 3.6 and Figure 3.7.

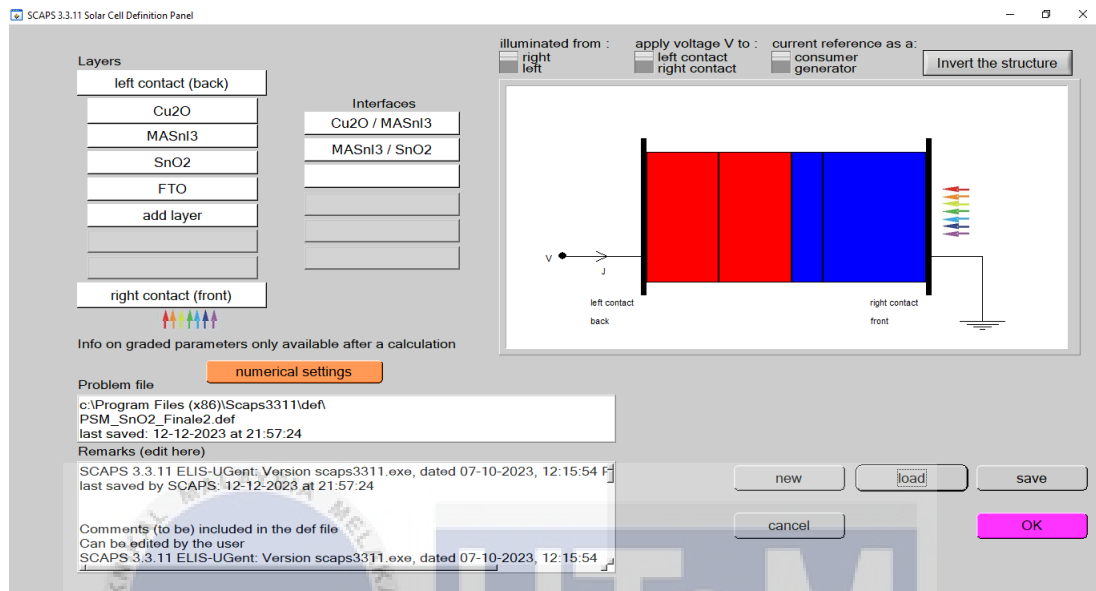


Figure 3.6: Simulated PSC structure (MASnI3) with SnO2 (ETL).

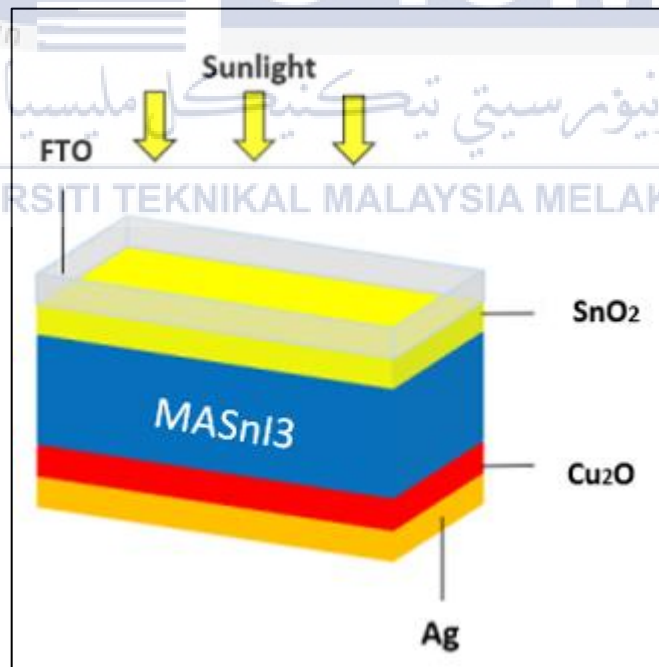


Figure 3.7: PSC Solar cell structure with SnO2 (ETL).

Improving the efficiency of perovskite solar cells (PSC) is a central goal of this study. The optimization strategies are strongly focused on specific attributes related to MASnI<sub>3</sub> and include factors such as the thickness of the absorber, the doping density, the operating temperature of the photovoltaic cell and the presence of a defect interface. These carefully considered parameters collectively contribute to the differentiated exploration and improvement of PSC efficiency within the SSDSSC device. By examining the differentiated properties of MASnI<sub>3</sub>, this study attempts to unravel the complex interplay of material properties and operating conditions, paving the way for advances in high-performance solar energy conversion technologies.

Table 3.1 contains a comprehensive compilation of the input parameters essential for performing numerical analyzes on the structural aspects of perovskite solar cells (PSC), whose parameter attributes are related to TiO<sub>2</sub>, MASnI<sub>3</sub>, Cu<sub>2</sub>O and FTO components for analysis using Include TiO<sub>2</sub> as ETL. Table 3.2 presents the input parameters for the analysis with SnO<sub>2</sub> as ETL.

Table 3.1 Input parameters of numerical analyzing the PSC using TiO<sub>2</sub> (ETL).

Parameter	<b>FTO</b> [32]	<b>TiO<sub>2</sub></b> [33][34]	<b>MASnI<sub>3</sub></b> [35]	<b>Cu<sub>2</sub>O</b> [36][37]
Layer thickness, d ( $\mu\text{m}$ )	0.5	0.05	0.350	0.35
Bandgap energy, E <sub>g</sub> (eV)	3.5	3.26	1.3	2.17
Electron affinity, (eV)	4	4	4.1	3.2
Dielectric permittivity, $\epsilon$ (relative)	9	32	8.2	7.11
Conduction Band density of states, N <sub>C</sub> ( $\text{cm}^{-3}$ )	$2.2 \times 10^{18}$	$1 \times 10^{19}$	$1 \times 10^{18}$	$2.02 \times 10^{17}$

Valence Band density of states, $N_V$ ( $\text{cm}^{-3}$ )	$1.8 \times 10^{19}$	$1 \times 10^{19}$	$1 \times 10^{18}$	$1.1 \times 10^{19}$
Electron thermal velocity, $V_e$ (cm/s)	$1 \times 10^7$	$1 \times 10^7$	$1 \times 10^7$	$1 \times 10^7$
Hole thermal velocity, $V_h$ (cm/s)	$1 \times 10^7$	$1 \times 10^7$	$1 \times 10^7$	$1 \times 10^7$
Electron mobility, $\mu_e$ ( $\text{cm}^2/\text{Vs}$ )	20	20	1.6	20
Hole mobility, $\mu_h$ ( $\text{cm}^2/\text{Vs}$ )	10	10	1.6	80
Density of donor, $N_D$ ( $\text{cm}^{-3}$ )	$2.0 \times 10^{19}$	$1 \times 10^{17}$	0	0
Density of acceptor, $N_A$ ( $\text{cm}^{-3}$ )	0	0	$1 \times 10^{18}$	$1 \times 10^{18}$

Table 3.2: Input parameters of numerical analyzing the PSC using SnO<sub>2</sub> (ETL)

Parameter	FTO [32]	SnO <sub>2</sub> [38]	MASnI <sub>3</sub> [35]	Cu <sub>2</sub> O [36][37]
Layer thickness, $d$ ( $\mu\text{m}$ )	0.5	0.15	0.350	0.35
Bandgap energy, $E_g$ (eV)	3.5	3.5	1.3	2.17
Electron affinity, (eV)	4	4	4.1	3.2
Dielectric permittivity, $\epsilon$ (relative)	9	9	8.2	7.11
Conduction Band density of states, $N_C$ ( $\text{cm}^{-3}$ )	$2.2 \times 10^{18}$	$2.2 \times 10^{17}$	$1 \times 10^{18}$	$2.02 \times 10^{17}$
Valence Band density of states, $N_V$ ( $\text{cm}^{-3}$ )	$1.8 \times 10^{19}$	$2.2 \times 10^{16}$	$1 \times 10^{18}$	$1.1 \times 10^{19}$
Electron thermal velocity, $V_e$ (cm/s)	$1 \times 10^7$	$1 \times 10^7$	$1 \times 10^7$	$1 \times 10^7$
Hole thermal velocity, $V_h$ (cm/s)	$1 \times 10^7$	$1 \times 10^7$	$1 \times 10^7$	$1 \times 10^7$
Electron mobility, $\mu_e$ ( $\text{cm}^2/\text{Vs}$ )	20	20	1.6	20
Hole mobility, $\mu_h$ ( $\text{cm}^2/\text{Vs}$ )	10	10	1.6	80

Density of donor, ND (cm <sup>-3</sup> )	2.0 x 10 <sup>19</sup>	1 x 10 <sup>17</sup>	0	0
Density of acceptor, NA (cm <sup>-3</sup> )	0	0	1 x 10 <sup>18</sup>	1 x 10 <sup>18</sup>

### 3.3.3 Method of Analysis

Exploring optimal efficiency in perovskite solar cells (PSC) requires in-depth study of critical parameter values associated with MASnI<sub>3</sub> as an absorber. Key considerations include examining the thickness of MASnI<sub>3</sub>, the doping density of TiO<sub>2</sub>/SnO<sub>2</sub> and Cu<sub>2</sub>O, the operating temperature of the solar cell, and the possible effects of a defect interface between each layer. These parameters play a crucial role in determining the overall performance and efficiency of the PSC and highlight the need for a thorough analysis and understanding of their respective influences.

#### 3.3.3.1 Analysis of the variation of Temperature

The effectiveness of electricity conversion in solar cells is directly influenced by the working temperature. This analysis spans a temperature range of 300K to 500K to determine the most favorable power conversion performance for PSC, with temperatures expressed in Kelvin.

#### 3.3.3.2 Analysis of the variation of Thickness

The analysis of the thickness of the MASnI<sub>3</sub> absorber involves changing the thickness of the layers within the same structure. In this study, only the layers connected to the absorber are adjusted for each simulation.



### 3.3.3.3 Analysis of the variation of Doping density

Typically, higher doping levels result in reduced conductivity due to the increased carrier concentration. The doping density is concentrated in the electron transport layer (ETL) and the hole transport layer (HTL). Specifically, the N-type (ND) doping is introduced into the ETL layer, while the P-type (NA) doping is introduced into the HTL layer. In this analysis, the values of ND and NA were adjusted in the range of  $10^{15}$  to  $10^{20}$   $\text{cm}^{-3}$  and  $10^{12}$  to  $10^{17}$   $\text{cm}^{-3}$  respectively.

### 3.3.3.4 Analysis of the variation of Defect density

This study focused exclusively on a single type of interface with defect density, particularly the neutral interface. The investigation focused on a proposed single defect interface layer, which is the defect that occurs at the interface between the ETL and absorber layers. The overall interfacial defect density when integrated over all energies ranged from  $10^{15}$  to  $10^{20}$   $\text{cm}^{-2}$  for MASnI3 / TiO2 and  $10^{12}$  to  $10^{17}$   $\text{cm}^{-2}$  for MASnI3 / SnO2.

## CHAPTER 4:

### RESULTS AND DISCUSSION



This section will delve into the outcomes obtained and the underlying theoretical aspects pertinent to the successful completion of the project. The enhancement of solar cell performance and efficiency involves the careful observation and measurement of diverse characteristics.

#### 4.1 Analysis of MASnI3 and TiO2 (ETL)

The initial phase of the analysis involves performing a numerical simulation using the SCAPS-1D software. The focus of this simulation is to examine and optimize the parameters associated with each structured layer to achieve optimal efficiency. The main performance indicators considered and studied in this simulation include the efficiency ratio (PCE), open-circuit voltage ( $V_{oc}$ ), short-circuit current ( $J_{sc}$ ) and fill factor (FF) of the photovoltaic cell. These parameters are recorded and examined using the obtained current-voltage (J-V) curve.

##### 4.1.1 Analysis of working temperature I

The working temperature turns out to be a decisive factor that significantly influences the photovoltaic performance of lead-free PSC. In this simulation, the temperature values range from 300 K to 500 K with incremental steps of 20 K. Table 4.1 explains the constant parameter values used in creating the temperature diagram. The results of the lead-free PSC simulations, in the form of the data presented in Table 4.2 and the graphical representation in Figure 4.1, comprehensively included for thorough examination and analysis.

Table 4.1: Constant parameter value for working temperature analysis using TiO2.

Parameter	Cu2O	MASnI3	TiO2
Thickness ( $\mu\text{m}$ )	0.35	0.35	0.05
Doping Donor Density	0	0	$10^{17}$
Doping Acceptor Density	$10^{18}$	$10^{18}$	0

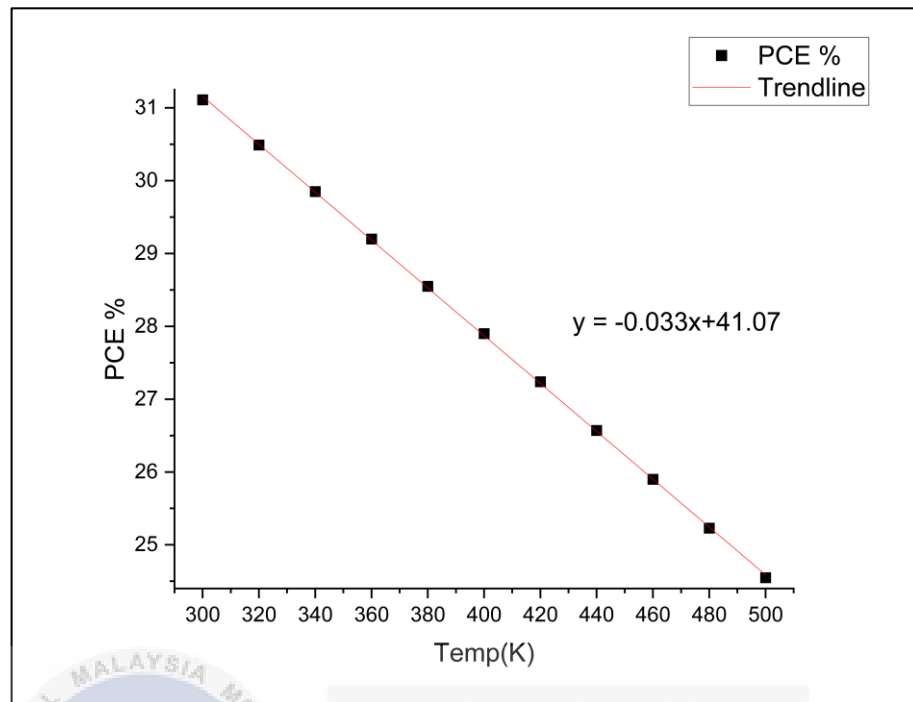


Figure 4.1: The analysis of efficiency based on the variation of working temperature using TiO<sub>2</sub>.

Table 4.2: The analysis of efficiency based on the variation of working temperature using TiO<sub>2</sub>.

Working Temperature (K)	Voc	Jsc	FF (%)	PCE (%)
300	1.163	30.069	89.01	31.11
320	1.147	30.081	88.36	30.49
340	1.131	30.091	87.69	29.85
360	1.115	30.101	87.01	29.20
380	1.099	30.110	86.30	28.55
400	1.082	30.118	85.61	27.90
420	1.065	30.125	84.91	27.24
440	1.047	30.132	84.19	26.57
460	1.030	30.139	83.46	25.90
480	1.012	30.145	82.72	25.23
500	0.994	30.151	81.96	24.55

According to the observations in Figure 4.1, as the operating temperature increases, there is a downward trend in the efficiency of the solar cell, with a slope of -0.033% per Kelvin. Notably, all parameters except short-circuit current ( $J_{sc}$ ) show a steady decrease in response to increased temperatures, and even  $J_{sc}$  shows only a slight increase. This trend is attributed to the significant influence of higher temperatures on the carrier concentration, charge mobility, resistance and band gap of the material, which overall leads to a shift in the fundamental properties of the photovoltaic (PV) system [39]. The increased charge carrier concentration in the semiconductor induced by an increased operating temperature significantly accelerates the rate of internal charge carrier recombination. Furthermore, the open-circuit voltage ( $V_{oc}$ ) experiences a reduction due to an increase in the reverse saturation current that accompanies the temperature increase. These complicated relationships highlight the connection between temperature and the key properties of the photovoltaic system and provide valuable insights for optimizing performance under different operating conditions.

#### 4.1.2 Analysis of the variation of MASnI3 thickness I

As part of this analysis, the thickness of MASnI3 is varied and is between 0.1  $\mu\text{m}$  to 1  $\mu\text{m}$ . Table 4.3 provides a comprehensive overview of the fixed parameters used in creating the thickness diagram. Table 4.4 provides a detailed representation of the simulated absorber thickness data extracted from the results. Overall, these tables serve as essential references for understanding the impact of MASnI3 thickness on the performance of the system and provide insight into the nuanced relationships between thickness variations and key parameters.

Table 4.3: The constant set parameter value for Absorber thickness analysis using TiO<sub>2</sub>.

Parameter	Cu <sub>2</sub> O	MASnI <sub>3</sub>	TiO <sub>2</sub>
Working Temperature (K)	300		
Thickness (μm)	0.35	<b>Varied</b>	0.05
Doping Donor Density (cm <sup>-3</sup> )	0	0	10 <sup>17</sup>
Doping Acceptor Density (cm <sup>-3</sup> )	10 <sup>18</sup>	10 <sup>18</sup>	0

Table 4.4: The analysis of efficiency based on the variation of absorber thickness using TiO<sub>2</sub>.

Absorber Thickness (μm)	Voc	Jsc	FF (%)	PCE (%)
0.1	1.179	18.405	88.69	19.24
0.2	1.171	25.193	88.96	26.24
0.3	1.165	28.882	89.01	29.95
0.4	1.160	30.970	89.00	31.98
0.5	1.156	32.191	89.01	33.11
0.6	1.152	32.921	89.00	33.75
0.7	1.149	33.362	88.97	34.09
0.8	1.146	33.626	88.93	34.26
0.9	1.143	33.779	88.89	34.33
1.0	1.141	33.861	88.85	34.34

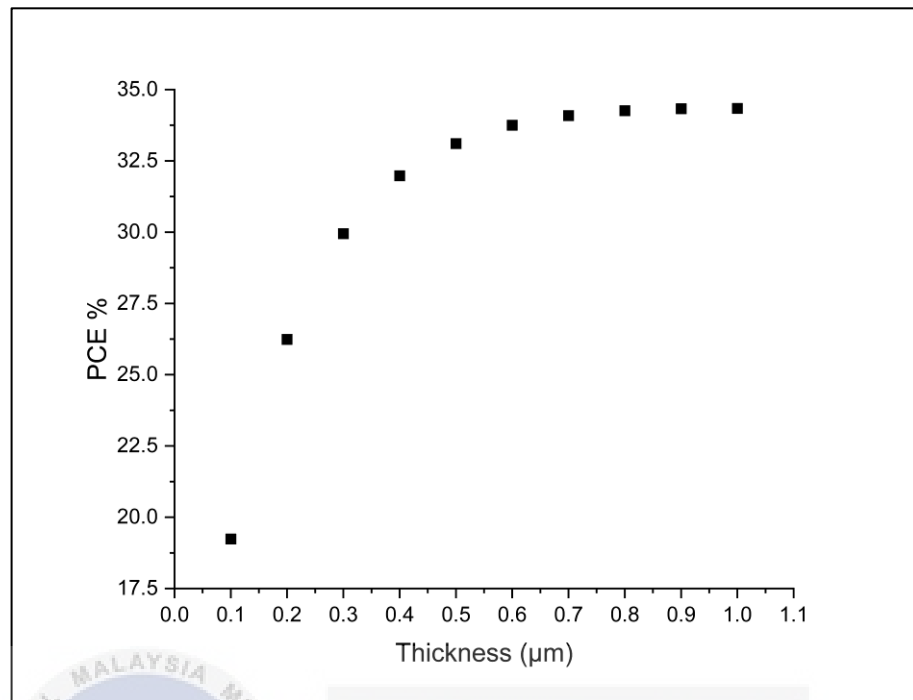


Figure 4.2: The analysis of efficiency based on the variation of absorber thickness using TiO<sub>2</sub>.

Considering the power conversion efficiency (PCE) in relation to the thickness of the absorber layer in micrometers ( $\mu\text{m}$ ) shows a convincing trend. Starting at 0.1  $\mu\text{m}$  with an initial PCE of 19.24%, a consistent and noticeable increase is observed with increasing absorber layer thickness. This increase continues and reaches 26.24% at 0.2  $\mu\text{m}$ , indicating a significant increase in efficiency with an expanded absorber layer. The upward trend persists and peaks at 34.34% at 1.0  $\mu\text{m}$ , indicating an optimal absorber layer thickness for maximum efficiency within the studied range. However, it is noteworthy that there is a significant diminishing return in PCE increase as we approach 1.0  $\mu\text{m}$ , highlighting the importance of carefully balancing the thickness for optimal solar cell performance.

The thickness of the absorber layer can be due to several interrelated factors that influence the performance of a solar cell. A thicker absorber layer allows for greater

absorption of sunlight, provides more opportunities for photon absorption, and creates a higher number of electron-hole pairs. This increase in short-circuit current ( $J_{sc}$ ) contributes positively to the overall PCE. Although a thicker absorber layer may result in a slight reduction in open circuit voltage ( $V_{oc}$ ), the net impact on PCE remains positive as the improvement in  $J_{sc}$  often outweighs the reduction in  $V_{oc}$ . In addition, the filling factor (FF), which represents efficient carrier transport, contributes to the overall improvement of the PCE. It is important to find a balance in absorber layer thickness as there is a point at which yields decrease and further increases may result in a plateau or reduction in efficiency due to factors such as increased recombination rates or optical losses. Therefore, optimizing absorber layer thickness is a crucial consideration for designing solar cells with maximum efficiency.

#### 4.1.3 Analysis of the variation of Doping donor density I

The investigation then shifts its focus to the variation of the doping donor density in the range from  $10^{15} \text{ cm}^{-3}$  to  $10^{20} \text{ cm}^{-3}$ . Table 4.5 illustrates the fixed parameters that are essential for the analysis and visualization of the doping donor density diagram. Table 4.6 then provides a comprehensive compilation and documentation of the data extracted through the simulation process. This dual tabular representation serves as a central reference point as it describes in detail both the constant parameters and the corresponding results derived from the simulation, allowing a thorough investigation of the influence of doping donor density on the properties of the solar cell system.



Table 4.5: The constant set parameters value for doping donor analysis using TiO<sub>2</sub>.

Parameter	Cu <sub>2</sub> O	MASnI <sub>3</sub>	TiO <sub>2</sub>
Working Temperature (K)	300		
Thickness (μm)	0.35	0.35	0.05
Doping Donor Density (cm <sup>-3</sup> )	0	0	<b>Varied</b>
Doping Acceptor Density (cm <sup>-3</sup> )	10 <sup>18</sup>	10 <sup>18</sup>	0

Table 4.6: Analysis of efficiency based on the variation of doping donor density using TiO<sub>2</sub>.

Doping Donor Density (cm <sup>-3</sup> )	Voc	Jsc	FF (%)	PCE (%)
10 <sup>15</sup>	1.163	30.067	89.17	31.18
10 <sup>16</sup>	1.163	30.067	89.16	31.18
10 <sup>17</sup>	1.163	30.069	89.01	31.11
10 <sup>18</sup>	1.162	30.079	88.53	30.93
10 <sup>19</sup>	1.162	30.086	88.52	30.94
10 <sup>20</sup>	1.162	30.087	88.53	30.94

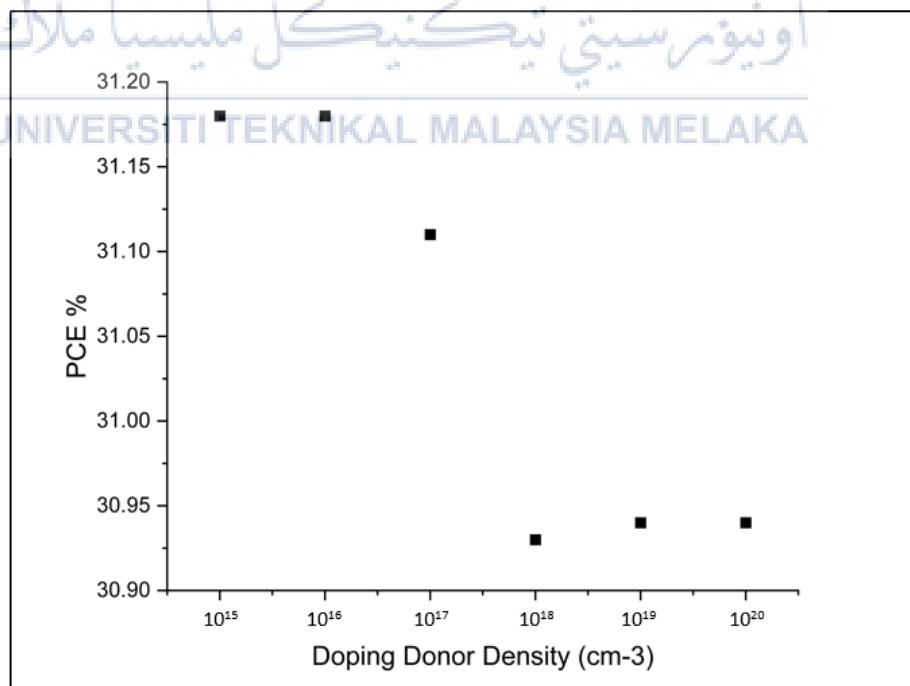


Figure 4.3: The analysis of efficiency based on the variation of doping donor density using TiO<sub>2</sub>.

The observation of power conversion efficiency (PCE) versus doping donor density (ND) in the electron transport layer (ETL) shown in Figure 4.3 shows a differentiated trend. As the donor density varies between  $10^{15} \text{ cm}^{-3}$  to  $10^{20} \text{ cm}^{-3}$ , the PCE gradually decreases, starting at 31.18% for  $\text{ND} = 10^{15}$  and slightly decreasing to 30.94% for  $\text{ND} = 10^{19}$  and  $10^{20}$ . This indicates a nonlinear relationship and the existence of an optimal range for the doping density that maximizes the PCE. Despite the variation in doping density, the open-circuit voltage ( $V_{oc}$ ) and short-circuit current ( $J_{sc}$ ) show small variations, suggesting limited effects within the studied range. However, the fill factor (FF) decreases slightly with increasing doping density, indicating that higher donor densities may contribute to a reduction in the FF and thus the overall efficiency of the solar cell. The observed PCE peak at  $\text{ND} = 10^{15}$  indicates an optimal doping density to achieve the highest efficiency and highlights the importance of carefully tuning the donor density in the ETL layer for optimal solar cell performance.

The decrease in power conversion efficiency (PCE) accompanied by an increase in doping donor density (ND) in the electron transport layer (ETL) can be attributed to several interrelated factors. Increased ND values can intensify carrier recombination within the ETL, reducing the number of effective carriers available for power generation and thereby reducing PCE [39]. Furthermore, higher doping densities can negatively impact carrier mobility and transport properties, leading to increased scattering and reduced mobility. In addition, excessive doping can lead to increased contact resistance and series resistance in the ETL, resulting in energy losses and further reduction in PCE. Changes in doping density can also alter the bandgap of the ETL material, affecting the absorption and utilization of sunlight and impacting the overall efficiency of the solar cell. Finally, higher doping concentrations can introduce

defects or impurities into the material, creating recombination centers that trap charge carriers and contribute to increased recombination rates, further impacting PCE. Therefore, optimizing the doping density is crucial to balance these factors and ensure the efficient performance of the solar cell.

#### 4.1.4 Analysis of the variation of Doping acceptor density I

In addition, the study focuses on studying the fluctuations of doping acceptor density in the range of  $10^{15} \text{ cm}^{-3}$  to  $10^{20}$ . The parameters that remain constant for the analysis and visualization of the doping acceptor density diagram are explained in Table 4.7. At the same time, Table 4.8 represents a comprehensive compilation and documentation of the data obtained from the simulation process. This dual tabular representation serves as a crucial reference point and describes both the invariant parameters and the corresponding results achieved through simulation. This setup enables a comprehensive investigation of how variations in the doping acceptor density influence the properties of the solar cell system.

Table 4.7: The constant set parameter value for doping acceptor analysis using TiO<sub>2</sub>.

Parameter	Cu <sub>2</sub> O	MA <sub>3</sub> SnI <sub>3</sub>	TiO <sub>2</sub>
Working Temperature (K)	300		
Thickness ( $\mu\text{m}$ )	0.35	0.35	0.05
Doping Donor Density ( $\text{cm}^{-3}$ )	0	0	$10^{17}$
Doping Acceptor Density ( $\text{cm}^{-3}$ )	<b>Varied</b>	$10^{18}$	0

Table 4.8: Analysis of efficiency based on the variation of doping acceptor density using TiO<sub>2</sub>.

Doping Acceptor Density (cm <sup>-3</sup> )	Voc	Jsc	FF (%)	PCE (%)
10 <sup>15</sup>	1.162	29.926	88.97	30.94
10 <sup>16</sup>	1.162	29.967	88.98	30.98
10 <sup>17</sup>	1.162	30.041	88.99	31.07
10 <sup>18</sup>	1.163	30.069	89.01	31.11
10 <sup>19</sup>	1.163	30.080	89.03	31.15
10 <sup>20</sup>	1.164	30.085	89.03	31.17

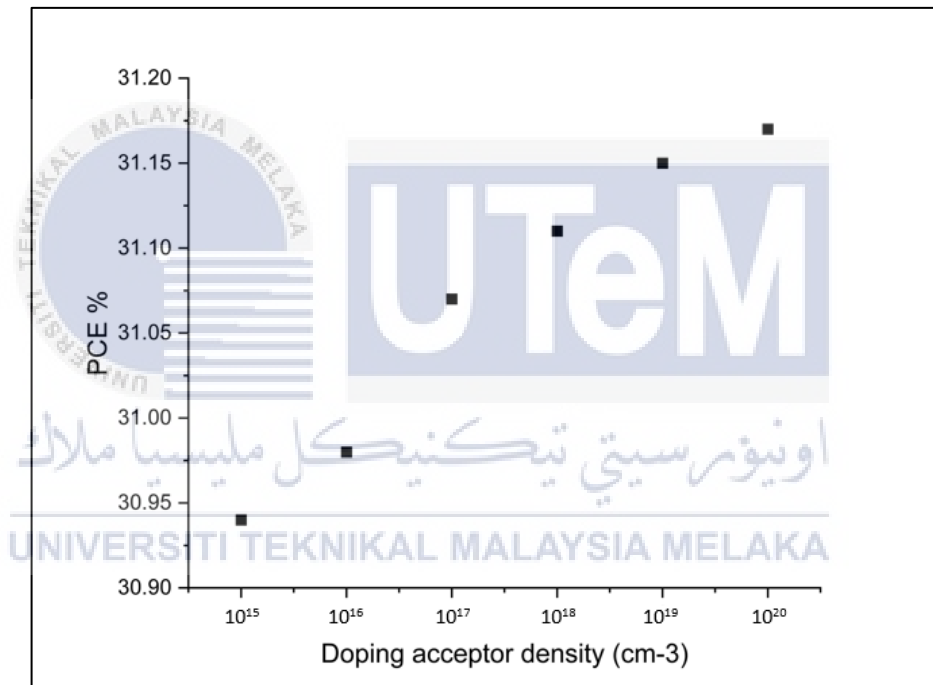


Figure 4.4: The analysis of efficiency based on the variation of doping acceptor density using TiO<sub>2</sub>.

The results shown in Figure 4.4 provide a comprehensive insight into the interplay between power conversion efficiency (PCE) and dopant acceptor density (NA) within the hole transport layer (HTL). A noticeable trend emerges when the acceptor density varies between 10<sup>15</sup> cm<sup>-3</sup> to 10<sup>20</sup> cm<sup>-3</sup>, indicating a gradual increase in PCE. Starting at 30.94% for NA = 10<sup>15</sup>, the efficiency increases steadily and reaches 31.17% for NA = 10<sup>20</sup>. This positive correlation highlights the influence of the acceptor density on the

overall efficiency of the solar cell. Examination of other parameters shows that the open-circuit voltage ( $V_{oc}$ ) exhibits a slight increase, suggesting that higher acceptor densities contribute to a higher voltage potential. Short-circuit current ( $J_{sc}$ ) shows an upward trend, meaning increased acceptor density allows greater current flow, improving overall efficiency. Furthermore, the fill factor (FF) improves with increasing acceptor density, indicating more efficient use of the generated charge carriers. The data suggests that within the studied range, the optimal efficiency is achieved at  $NA = 10^{20}$ , highlighting the need for careful optimization of the doping acceptor density for maximum solar cell performance.

The increase in power conversion efficiency (PCE) with an increase in dopant acceptor density (NA) within the hole transport layer (HTL) can be explained by several interdependent factors. First, the increased acceptor density leads to an increased concentration of charge carriers, especially holes, within the HTL. This increased carrier concentration enables more efficient hole transport and contributes to a higher short-circuit current ( $J_{sc}$ ) and thus increased PCE. Furthermore, the increase in acceptor density is often accompanied by an increased fill factor (FF), indicating a reduction in resistive losses and further contributing to the overall increase in PCE. Changes in the electrical properties of the HTL, influenced by higher acceptor density, play a role in optimizing conductivity and minimizing contact resistance [40]. This in turn has a positive effect on the efficiency of the solar cell.

The increased acceptor density also helps balance charge extraction and reduce charge recombination within the HTL, promoting effective hole extraction and contributing to improvements in both  $J_{sc}$  and PCE. While the open circuit voltage ( $V_{oc}$ ) may exhibit minor fluctuations, it further contributes to the overall improvement

of the PCE. It is crucial to recognize the existence of an optimal range for doping acceptor density, beyond which further increases may result in diminishing returns or even a decrease in efficiency. Therefore, careful optimization is of utmost importance to strike a balance between improved charge transport and potential adverse effects associated with excessively high doping levels, such as increased resistive losses or recombination rates.

#### 4.1.5 Analysis of the variation of Defect density at the interface I

Moreover, the investigation focuses on the targeted variation of the defect density at the MASnI3/TiO2 interface and examines a spectrum in the range from  $10^{15}$  to  $10^{20}$   $\text{cm}^{-2}$ . Figure 4.5 carefully illustrates the graphical representation of defect density for the device and provides a visual representation of the relationship between defect density and the characteristics of the device. At the same time, Table 4.9 carefully presents the invariant values that were used as constants throughout the analysis to ensure a robust and consistent framework for evaluation. As we delve deeper into the efficiency analysis, Table 4.10 serves as a comprehensive reference and presents a nuanced examination of how different defect densities at the MASnI3/TiO2 interface affect the overall efficiency of the device.

Table 4.9: The constant set parameter value for defect density analysis using TiO2.

Parameter	Cu2O	MASnI3	TiO2
Working Temperature (K)	300		
Thickness ( $\mu\text{m}$ )	0.35	0.35	0.05
Doping Donor Density ( $\text{cm}^{-3}$ )	0	0	$10^{17}$
Doping Acceptor Density ( $\text{cm}^{-3}$ )	$10^{18}$	$10^{18}$	0

Table 4.10: Analysis of efficiency based on the variation of defect density at MASnI3/TiO2.

Doping Defect Density ( $\text{cm}^{-2}$ )	Voc	Jsc	FF (%)	PCE (%)
$10^{15}$	0.893	30.068	77.87	20.91
$10^{16}$	0.770	30.064	75.02	17.36
$10^{17}$	0.649	30.026	73.20	14.27
$10^{18}$	0.562	29.877	73.31	12.31
$10^{19}$	0.540	29.795	73.00	11.75
$10^{20}$	0.538	29.756	72.92	11.68

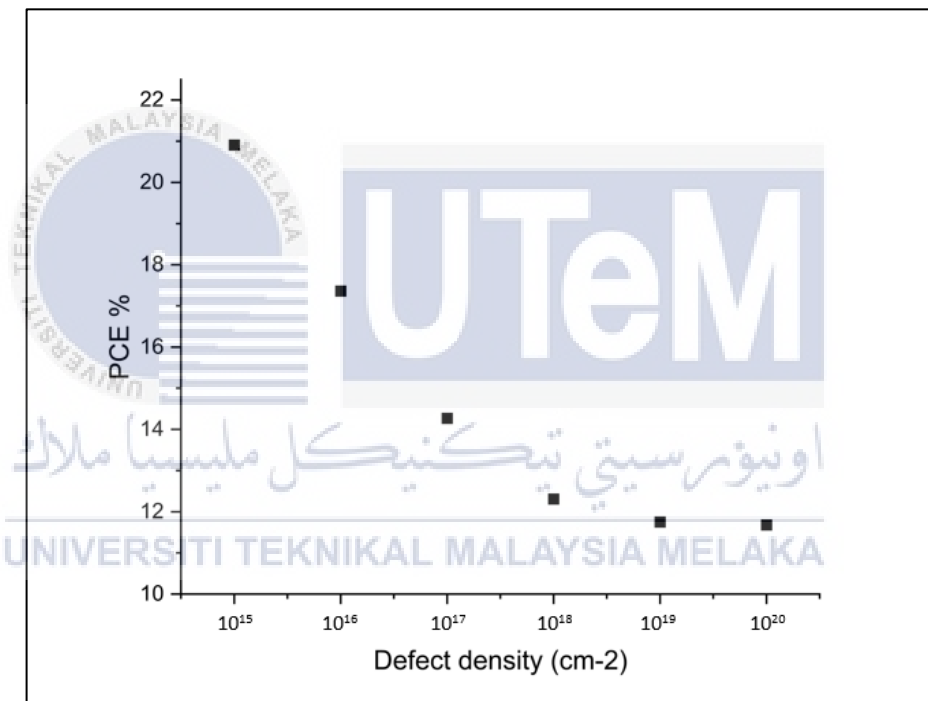


Figure 4.5: Analysis for the variation of defect density at MASnI3/TiO2.

The obtained data enables a comprehensive study of the complex relationship between the power conversion efficiency (PCE) and the doping defect density within the solar cell. The PCE trend is clearly observed as the defect density varies between  $10^{15}$  to  $10^{20} \text{ cm}^{-2}$ . Starting from a PCE of 20.91% for  $10^{15}$ , the efficiency gradually decreases and reaches 11.68% for  $10^{20}$ . This continuous decline suggests a reciprocal correlation between defect density and PCE, meaning that higher defect densities have

a negative impact on overall efficiency of the solar cell. Analysis of the relationship with other parameters shows that the open-circuit voltage ( $V_{oc}$ ) steadily decreases with increasing defect density, indicating increased charge recombination and reduced power generation potential. The short-circuit current ( $J_{sc}$ ) experiences a slight decrease, which contributes to the overall reduction in PCE. At the same time, the fill factor (FF) gradually decreases, reflecting an increase in resistance losses within the solar cell. The data highlight the importance of minimizing defect density for optimal solar cell performance and highlight the need for strategies to mitigate charge recombination and resistive losses to improve overall efficiency.

The decrease in power conversion efficiency (PCE) with increasing doping defect density can be explained by a combination of interrelated factors within the solar cell system. Higher defect densities lead to additional recombination centers, resulting in increased charge recombination and loss of charge carriers before they contribute to the generated current [41]. This increased recombination has a negative impact on the overall efficiency of the solar cell. Furthermore, the increased defect densities can hinder the mobility of charge carriers, reducing their effective movement within the solar cell and leading to lower short-circuit current ( $J_{sc}$ ). Furthermore, the increase in defect density contributes to increased resistive losses, hindering current flow and leading to a decrease in fill factor (FF), further reducing efficiency. Changes in the electrical properties of materials due to higher defect densities can affect parameters such as open-circuit voltage ( $V_{oc}$ ), affecting the potential for power generation. In addition, defects can affect the optical properties of materials and their ability to absorb and transmit light, thereby affecting the efficiency of the photovoltaic conversion process. It is important to consider a threshold for error saturation because,



at a certain point, the negative impact of errors may outweigh the potential benefits, resulting in a reduction in PCE. Essentially, optimizing solar cell performance is about finding a delicate balance to minimize defect density while maximizing other crucial performance factors.

## 4.2 Analysis of MASnI<sub>3</sub> and SnO<sub>2</sub> (ETL)

The first phase of the analysis involves performing a numerical simulation with SCAPS-1D software for solar cells using MASnI<sub>3</sub> as absorber and SnO<sub>2</sub> as ETL. This simulation is used to explore and refine the parameters of each structured layer to achieve optimal efficiency. The main focus of this simulation is to evaluate key performance indicators such as photovoltaic cell efficiency (PCE), open circuit voltage (Voc), short circuit current (Jsc) and fill factor (FF). These parameters are carefully recorded and examined using the current-voltage (J-V) curve obtained from the simulation.

### 4.2.1 Analysis of working temperature II

The working temperature plays a crucial role in shaping the photovoltaic performance of lead-free perovskite solar cells (PSC). In the context of this simulation, the temperature varies over a spectrum from 300 K to 500 K with incremental steps of 20 K. Table 4.11 provides clarity on the constant parameter values used in constructing the temperature diagram. The results derived from the lead-free PSC simulations, consisting of the data listed in Table 4.12 and visually represented in Figure 4.6, are thoroughly considered for comprehensive testing and analysis.

Table 4.11: Constant parameter value for working temperature analysis using SnO<sub>2</sub>.

Parameter	Cu <sub>2</sub> O	MASnI <sub>3</sub>	SnO <sub>2</sub>
Thickness (μm)	0.35	0.35	0.15
Doping Donor Density	0	0	10 <sup>17</sup>
Doping Acceptor Density	10 <sup>18</sup>	10 <sup>18</sup>	0

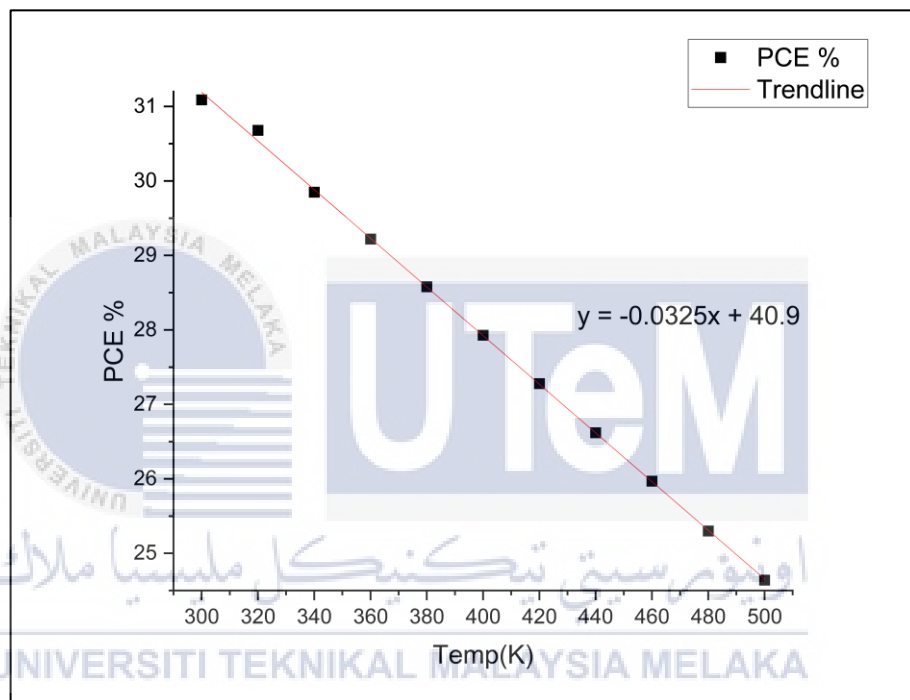


Figure 4.6: The analysis of efficiency based on the variation of working temperature using SnO<sub>2</sub>.

Table 4.12: The analysis of efficiency based on the variation of working temperature using SnO<sub>2</sub>.

Working Temperature (K)	Voc	Jsc	FF (%)	PCE (%)
300	1.163	29.936	89.30	31.09
320	1.147	29.949	88.68	30.68
340	1.132	29.961	88.04	29.85
360	1.116	29.971	87.37	29.22
380	1.100	29.980	86.69	28.58
400	1.083	29.989	86.03	27.93
420	1.066	29.997	85.36	27.28
440	1.048	30.004	84.67	26.62
460	1.031	30.010	83.96	25.97
480	1.013	30.016	83.25	25.30
500	0.995	30.022	82.52	24.64

As shown in Figure 4.6, the solar cell efficiency follows a significant downward trend with increasing operating temperature and has a slope of -0.0325% per Kelvin. What is noteworthy is the continuous decrease in all parameters, with the exception of the short-circuit current (Jsc), which only shows a slight increase at higher temperatures. This observed pattern is attributed to the significant influence of elevated temperatures on critical aspects such as carrier concentration, charge mobility, resistance and band gap of the material. Taken together, these factors lead to a fundamental change in the properties of the photovoltaic (PV) system [42]. The increased charge carrier concentration in the semiconductor induced by elevated operating temperatures significantly accelerates the rate of internal charge carrier recombination. In addition, the open circuit voltage (Voc) experiences a decrease due to an increase in reverse saturation current associated with the temperature increase. These complicated relationships illustrate the connection between temperature and the

critical properties of the photovoltaic system and provide valuable insights for optimizing performance under different operating conditions.

#### 4.2.2 Analysis of the variation of MASnI3 thickness II

In this analysis, where SnO<sub>2</sub> was used as ETL, the thickness of MASnI<sub>3</sub> varies in the range of 0.1  $\mu\text{m}$  to 1  $\mu\text{m}$ . A detailed overview of the constant parameters used in creating the thickness diagram is presented in Table 4.13, while Table 4.14 carefully presents the simulated absorber thickness data derived from the results. Together, these tables serve as important references for understanding the impact of MASnI<sub>3</sub> thickness on the overall system performance and illustrate the nuanced relationships between thickness variations and key system parameters.

Table 4.13: The constant set parameter value for absorber thickness analysis using SnO<sub>2</sub>.

Parameter	Cu <sub>2</sub> O	MASnI <sub>3</sub>	SnO <sub>2</sub>
Working Temperature (K)	300		
Thickness ( $\mu\text{m}$ )	0.35	<b>Varied</b>	0.15
Doping Donor Density ( $\text{cm}^{-3}$ )	0	0	$10^{17}$
Doping Acceptor Density ( $\text{cm}^{-3}$ )	$10^{18}$	$10^{18}$	0

Table 4.14: The analysis of efficiency based on the variation of absorber thickness using SnO<sub>2</sub>.

Absorber Thickness ( $\mu\text{m}$ )	Voc	Jsc	FF (%)	PCE (%)
0.1	1.180	18.296	89.31	19.27
0.2	1.172	25.076	89.37	26.25
0.3	1.166	28.755	89.33	29.94
0.4	1.161	30.832	89.26	31.94
0.5	1.156	32.042	89.24	33.06
0.6	1.152	32.761	89.21	33.67
0.7	1.149	33.192	89.17	34.00
0.8	1.146	33.447	89.13	34.16
0.9	1.144	33.591	89.08	34.22
1.0	1.142	33.664	89.03	34.21

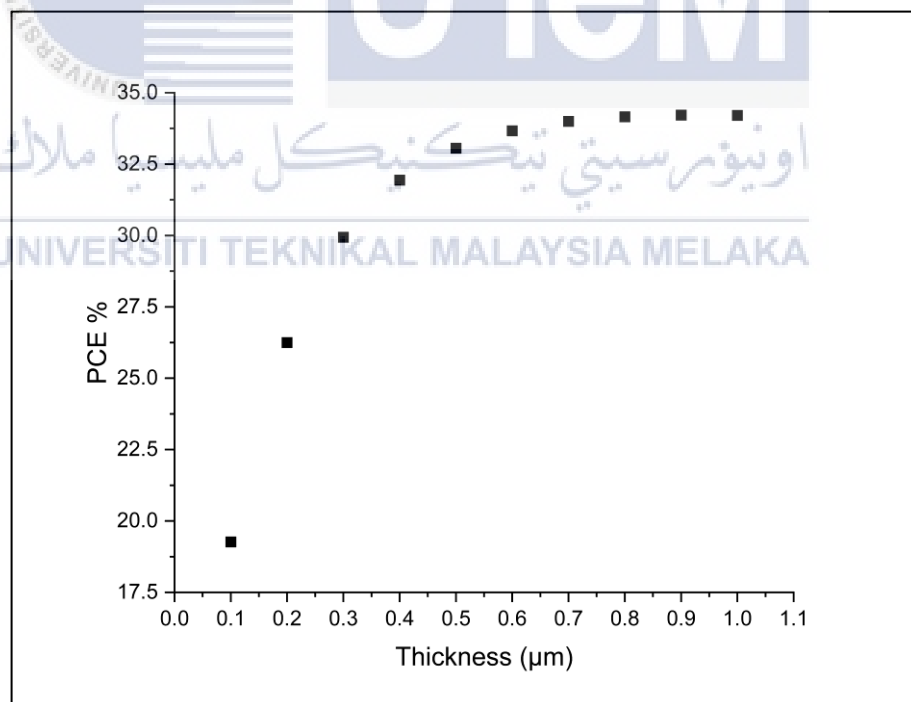


Figure 4.7: The analysis of efficiency based on the variation of absorber thickness using SnO<sub>2</sub>.

Figure 4.7 shows that the study of the power conversion efficiency (PCE) in terms of the thickness of the absorber layer in micrometers ( $\mu\text{m}$ ) shows a notable trend. Starting at  $0.1 \mu\text{m}$  with an initial PCE of 19.27%, there is a consistent and noticeable increase as the absorber layer thickness increases. This increase remains and reaches 26.25% at  $0.2 \mu\text{m}$ , which means a significant increase in efficiency with an expanded absorber layer. The upward trend continues and reaches a peak of 34.21% at  $1.0 \mu\text{m}$ , indicating an optimal absorber layer thickness for maximum efficiency within the studied range. However, as the thickness approaches  $1.0 \mu\text{m}$ , there is a significantly lower return on PCE increase, highlighting the importance of careful thickness balancing for optimal solar cell performance.

The enhancement of power conversion efficiency (PCE) with increasing absorber layer thickness can be attributed to several interrelated factors that affect the performance of solar cells. A thicker absorber layer allows for greater absorption of sunlight, creating more opportunities for photon absorption and creating a higher number of electron-hole pairs. This increase in short-circuit current ( $J_{sc}$ ) contributes positively to the overall PCE. While a thicker absorber layer may result in a slight reduction in open circuit voltage ( $V_{oc}$ ), the net impact on PCE remains positive, with the improvement in  $J_{sc}$  often outweighing the reduction in  $V_{oc}$ . In addition, the fill factor (FF), indicative of efficient charge carrier transport, contributes to the overall improvement in PCE. Striking a balance in absorber layer thickness is crucial, as there exists a point of diminishing returns where further increases may result in a plateau or decrease in efficiency due to factors like increased recombination rates or optical losses. Therefore, optimizing absorber layer thickness is a critical consideration for designing solar cells with maximum efficiency.

### 4.2.3 Analysis of the variation of Doping donor density II

The investigation then focuses on the variation of the doping donor density in the range from  $10^{12} \text{ cm}^{-3}$  to  $10^{17} \text{ cm}^{-3}$ . Table 4.15 illustrates the fixed parameters that are essential for the analysis and visualization of the doping donor density diagram. Table 4.16 then provides a comprehensive compilation and documentation of the data extracted through the simulation process. This dual tabular representation serves as a central reference point as it describes in detail both the constant parameters and the corresponding results derived from the simulation, allowing a thorough investigation of the influence of doping donor density on the properties of the solar cell system.

Table 4.15: The constant set parameters value for doping donor analysis using SnO<sub>2</sub>.

Parameter	Cu <sub>2</sub> O	MA <sub>2</sub> SnI <sub>3</sub>	SnO <sub>2</sub>
Working Temperature (K)	300		
Thickness ( $\mu\text{m}$ )	0.35	0.35	0.15
Doping Donor Density ( $\text{cm}^{-3}$ )	0	0	<b>Varied</b>
Doping Acceptor Density ( $\text{cm}^{-3}$ )	$10^{18}$	$10^{18}$	0

Table 4.16: Analysis of efficiency based on the variation of doping donor density using SnO<sub>2</sub>.

Doping Donor Density ( $\text{cm}^{-3}$ )	Voc	Jsc	FF (%)	PCE (%)
$10^{12}$	1.164	29.916	88.22	30.71
$10^{13}$	1.164	29.916	88.22	30.71
$10^{14}$	1.164	29.916	88.23	30.71
$10^{15}$	1.164	29.917	88.30	30.73
$10^{16}$	1.163	29.925	88.75	30.90
$10^{17}$	1.163	29.936	89.30	31.09

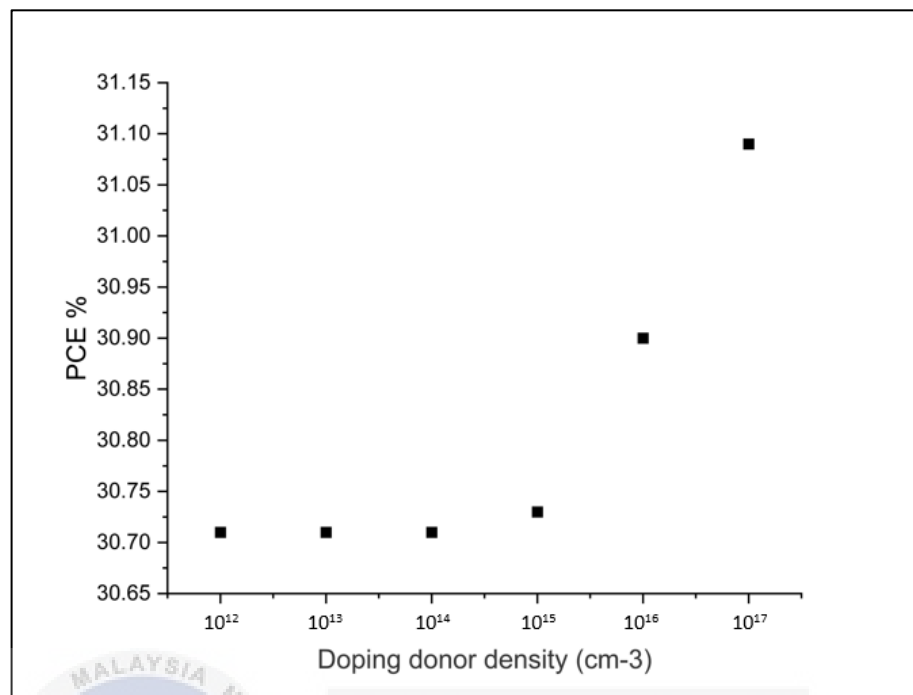


Figure 4.8: The analysis of efficiency based on the variation of doping donor density using SnO<sub>2</sub>.

The obtained data provides a detailed insight into the influence of doping donor density on the power conversion efficiency (PCE) of the electron transport layer (ETL), which is SnO<sub>2</sub>. The results show a consistent upward trend in PCE with increasing donor density, starting at 10<sup>12</sup> with a value of 30.71% and peaking at 31.09% for 10<sup>17</sup>. This positive correlation means that higher donor density contributes to improved PCE. Examining the relationships with other parameters, the open-circuit voltage (V<sub>oc</sub>) shows a slight increase with higher donor density, which has a positive effect on the PCE. At the same time, the short-circuit current (J<sub>sc</sub>) increases significantly, which makes a significant contribution to the overall improvement of the PCE. The fill factor (FF) also improves with increasing donor density, indicating more efficient charge carrier transport within the ETL layer. Overall, the data suggest that there is an optimal range for doping donor density that maximizes PCE, beyond which further increases may result in diminishing returns. These results provide



valuable insights into optimizing solar cell performance by carefully adjusting the doping donor density within the ETL layer.

#### 4.2.4 Analysis of the variation of Doping acceptor density II

In addition, the investigation now focuses on studying the variations in doping acceptor density, which covers a spectrum from  $10^{12} \text{ cm}^{-3}$  to  $10^{17} \text{ cm}^{-3}$ . Table 4.17 explains the parameters that remain consistent throughout the analysis and visualization of the dopant acceptor density plot. At the same time, Table 4.18 provides a comprehensive compilation and documentation of the data obtained from the simulation process. This dual tabular representation serves as a central reference point and describes both the parameters that remain unchanged, and the corresponding results derived from the simulation. Such a configuration enables a comprehensive study of the influence of variations in the doping acceptor density on the properties of the solar cell system.

Table 4.17: The constant set parameter value for doping acceptor analysis using SnO<sub>2</sub>.

Parameter	Cu <sub>2</sub> O	MASnI <sub>3</sub>	SnO <sub>2</sub>
Working Temperature (K)	300		
Thickness ( $\mu\text{m}$ )	0.35	0.35	0.15
Doping Donor Density ( $\text{cm}^{-3}$ )	0	0	$10^{17}$
Doping Acceptor Density ( $\text{cm}^{-3}$ )	<b>Varied</b>	$10^{18}$	0

Table 4.18: Analysis of efficiency based on the variation of doping acceptor density using SnO<sub>2</sub>.

Doping Acceptor Density (cm <sup>-3</sup> )	Voc	Jsc	FF (%)	PCE (%)
10 <sup>12</sup>	1.163	29.782	88.59	30.67
10 <sup>13</sup>	1.162	29.783	89.15	30.87
10 <sup>14</sup>	1.162	29.785	89.24	30.90
10 <sup>15</sup>	1.162	29.792	89.25	30.91
10 <sup>16</sup>	1.162	29.833	89.26	30.95
10 <sup>17</sup>	1.163	29.908	89.27	31.04

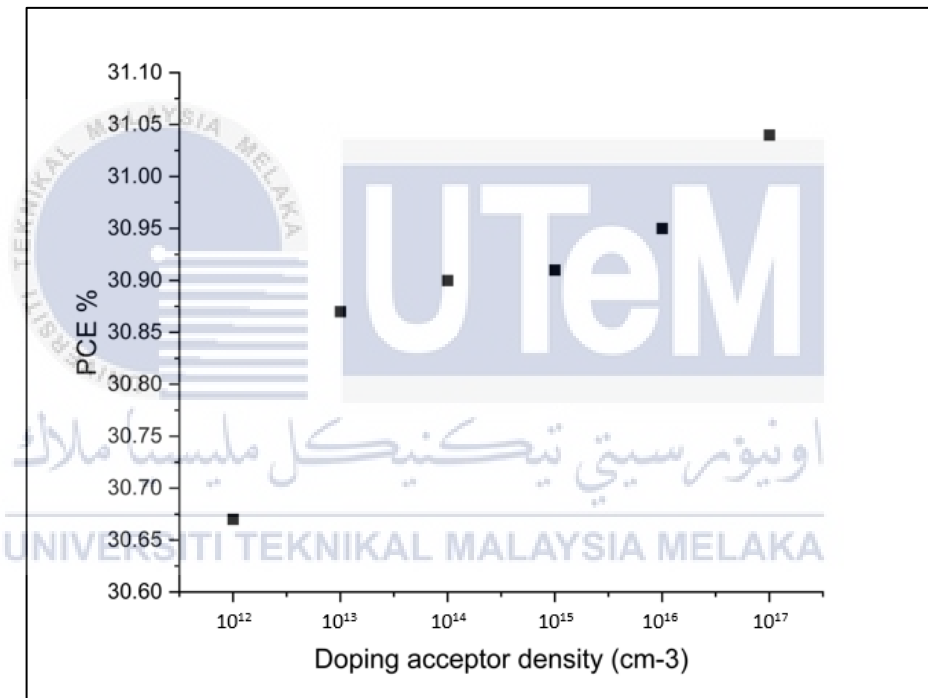


Figure 4.9: The analysis of efficiency based on the variation of doping acceptor density using SnO<sub>2</sub>.

The data obtained provides a comprehensive insight into the interplay between the power conversion efficiency (PCE) and the doping acceptor density (NA) within the hole transport layer (HTL). A noticeable trend emerges when the acceptor density varies between 10<sup>12</sup> cm<sup>-3</sup> to 10<sup>17</sup> cm<sup>-3</sup>, indicating a gradual increase in PCE. Starting at 30.67% for NA = 10<sup>12</sup>, the efficiency increases steadily and reaches 31.04% for NA

=  $10^{17}$ . This positive correlation highlights the influence of the acceptor density on the overall efficiency of the solar cell. Examination of other parameters shows that the open-circuit voltage ( $V_{oc}$ ) exhibits a slight increase, suggesting that higher acceptor densities contribute to a higher voltage potential. Short-circuit current ( $J_{sc}$ ) shows an upward trend, meaning increased acceptor density allows greater current flow, improving overall efficiency. Furthermore, the fill factor (FF) improves with increasing acceptor density, indicating more efficient use of the generated charge carriers. The data suggests that within the studied range, the optimal efficiency is achieved at  $NA = 10^{17}$ , highlighting the need for careful optimization of the doping acceptor density for maximum solar cell performance.

#### 4.2.5 Analysis of the variation of Defect density at the interface II

Other than that, the investigation focuses on the targeted variation of the defect density at the  $MASnI_3/SnO_2$  interface and examines a spectrum in the range from  $10^{12}$  to  $10^{17} \text{ cm}^{-2}$ . Figure 4.10 carefully illustrates the graphical representation of defect density for the device and provides a visual representation of the relationship between defect density and the characteristics of the device. At the same time, Table 4.19 carefully presents the invariant values that were used as constants throughout the analysis to ensure a robust and consistent framework for evaluation. As we delve deeper into the efficiency analysis, Table 4.20 serves as a comprehensive reference and presents a nuanced examination of how different defect densities at the  $MASnI_3/SnO_2$  interface affect the overall efficiency of the device.

Table 4.19: The constant set parameter value for defect density analysis using SnO<sub>2</sub>.

Parameter	Cu <sub>2</sub> O	MASnI <sub>3</sub>	SnO <sub>2</sub>
Working Temperature (K)	300		
Thickness (μm)	0.35	0.35	0.15
Doping Donor Density (cm <sup>-3</sup> )	0	0	10 <sup>17</sup>
Doping Acceptor Density (cm <sup>-3</sup> )	10 <sup>18</sup>	10 <sup>18</sup>	0

Table 4.20: Analysis of efficiency based on the variation of defect density at MASnI<sub>3</sub>/SnO<sub>2</sub>.

Doping Defect Density (cm <sup>-2</sup> )	Voc	Jsc	FF (%)	PCE (%)
10 <sup>12</sup>	1.161	29.934	89.14	30.97
10 <sup>13</sup>	1.143	29.915	88.47	30.47
10 <sup>14</sup>	1.090	29.725	87.40	28.32
10 <sup>15</sup>	1.024	27.949	83.91	24.02
10 <sup>16</sup>	0.958	17.486	71.80	12.02
10 <sup>17</sup>	0.891	3.690	63.18	2.08

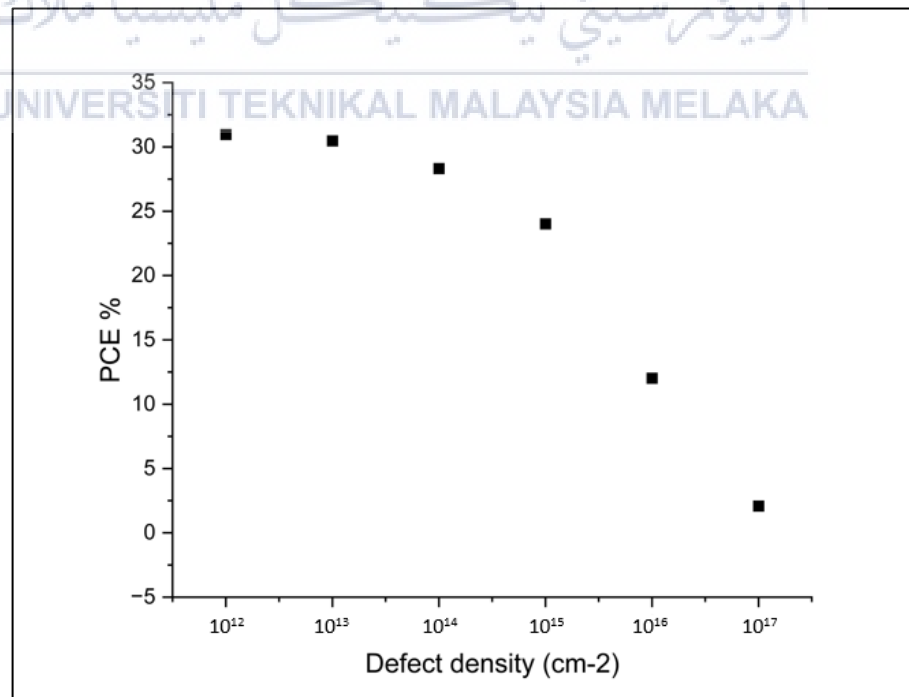


Figure 4.10: Analysis of the variation of defect density at MASnI<sub>3</sub>/SnO<sub>2</sub>.

Figure 4.10 shows the data revealing a detailed perspective on the interplay between the power conversion efficiency (PCE) and the doping defect density at the MASnI<sub>3</sub>/SnO<sub>2</sub> interface. The observed trend indicates a noticeable decrease in PCE with increasing defect density, starting at a value of 30.97% at 10<sup>12</sup> and decreasing to 2.08% at 10<sup>17</sup>. This demonstrates a clear negative correlation between defect density and PCE. Considering the relationships with other parameters, the open-circuit voltage (V<sub>oc</sub>) experiences a significant decrease with increasing defect density, contributing to the overall reduction in PCE. At the same time, the short-circuit current (J<sub>sc</sub>) decreases significantly, which further influences the decline of PCE. The fill factor (FF) also follows a decreasing trend with increased defect density, which contributes to the overall decline in PCE. The data suggests that there is an optimal defect density range that maximizes PCE and highlights the need for careful management to achieve optimal solar cell performance. These results provide valuable insights for researchers and engineers who want to improve the efficiency of solar cells by reducing and minimizing the defect density at the MASnI<sub>3</sub>/SnO<sub>2</sub> interface.

### **4.3 Analysis of efficiency based on optimum value for all parameters.**

#### **4.3.1 Analysis of the efficiency based on the optimization value for MASnI<sub>3</sub> as an absorber and TiO<sub>2</sub> as an ETL.**

Table 4.21 below shows the optimum value for all parameters achieved from the simulation analysis. The J-V curve of optimized PSC structure with TiO<sub>2</sub> as an ETL is shown in Figure 4.11.

Table 4.21: The optimized value for all parameters with TiO<sub>2</sub> as an ETL.

Parameter	FTO [32]	TiO <sub>2</sub> [33][34]	MASnI <sub>3</sub> [35]	Cu <sub>2</sub> O [36][37]
Layer thickness, d (μm)	0.5	0.05	*1	0.35
Bandgap energy, E <sub>g</sub> (eV)	3.5	3.26	1.3	2.17
Electron affinity, (eV)	4	4	4.1	3.2
Dielectric permittivity, ε (relative)	9	32	8.2	7.11
Conduction Band density of states, N <sub>C</sub> (cm <sup>-3</sup> )	2.2 x 10 <sup>18</sup>	1 x 10 <sup>19</sup>	1 x 10 <sup>18</sup>	2.02 x 10 <sup>17</sup>
Valence Band density of states, N <sub>V</sub> (cm <sup>-3</sup> )	1.8 x 10 <sup>19</sup>	1 x 10 <sup>19</sup>	1 x 10 <sup>18</sup>	1.1 x 10 <sup>19</sup>
Electron thermal velocity, V <sub>e</sub> (cm/s)	1 x 10 <sup>7</sup>	1 x 10 <sup>7</sup>	1 x 10 <sup>7</sup>	1 x 10 <sup>7</sup>
Hole thermal velocity, V <sub>h</sub> (cm/s)	1 x 10 <sup>7</sup>	1 x 10 <sup>7</sup>	1 x 10 <sup>7</sup>	1 x 10 <sup>7</sup>
Electron mobility, μ <sub>e</sub> (cm <sup>2</sup> /Vs)	20	20	1.6	20
Hole mobility, μ <sub>h</sub> (cm <sup>2</sup> /Vs)	10	10	1.6	80
Density of donor, N <sub>D</sub> (cm <sup>-3</sup> )	2.0 x 10 <sup>19</sup>	*1 x 10 <sup>15</sup>	0	0
Density of acceptor, N <sub>A</sub> (cm <sup>-3</sup> )	0	0	1 x 10 <sup>18</sup>	*1 x 10 <sup>20</sup>

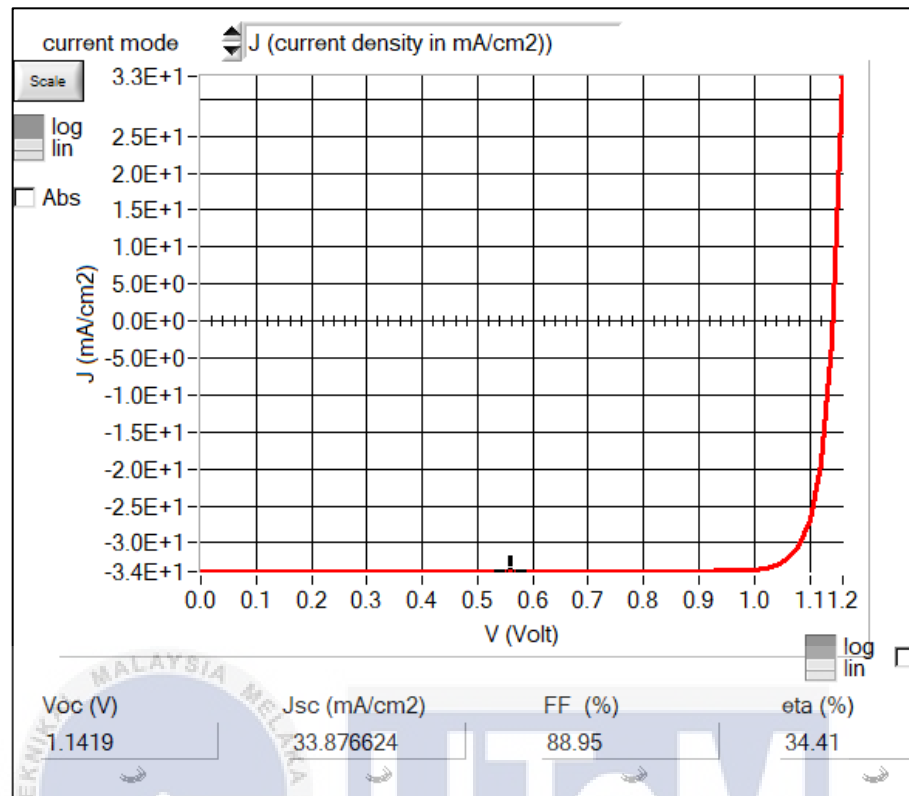


Figure 4.11: J-V curve for the optimized PSC structure using TiO<sub>2</sub> as an ETL.

The comprehensive analysis in Table 4.21 shows that integrating TiO<sub>2</sub> as an electron transport layer (ETL) gives optimal efficiency when all parameters are replaced with their respective optimal values. The simulation results show a remarkable Power Conversion Efficiency (PCE) of 34.41%, highlighting the significant improvement achieved. This improvement is further highlighted by a fill factor (FF) that reaches an impressive 88.95%, indicating improved efficiency of charge carrier transport within the solar cell. In addition, the open-circuit voltage (Voc) reaches a remarkable value of 1.142 V, highlighting the robust performance of the optimized structure. At the same time, the short-circuit current (Jsc) is 33.877 mA/cm<sup>2</sup>, which reflects the increased power generation in the solar cell. Overall, these results highlight the effectiveness of incorporating TiO<sub>2</sub> as ETL and MASnI<sub>3</sub> as absorber, showing not

only increased overall efficiency but also notable advances in each critical parameter, thereby contributing to optimizing the performance of perovskite solar cells (PSC).

#### 4.3.2 Analysis of the efficiency based on the optimization value for MASnI3 as an absorber and SnO2 as an ETL.

Table 4.22 below shows the optimum value for all parameters achieved from the simulation analysis. The J-V curve of optimized PSC structure with SnO2 as an ETL is shown in Figure 4.12.

Table 4.22: The optimized value for all parameters with SnO2 as an ETL.

Parameter	FTO [32]	SnO2 [38]	MASnI3 [35]	Cu2O [36][37]
Layer thickness, d ( $\mu\text{m}$ )	0.5	0.15	*1	0.35
Bandgap energy, $E_g$ (eV)	3.5	3.5	1.3	2.17
Electron affinity, (eV)	4	4	4.1	3.2
Dielectric permittivity, $\epsilon$ (relative)	9	9	8.2	7.11
Conduction Band density of states, $N_C$ ( $\text{cm}^{-3}$ )	$2.2 \times 10^{18}$	$2.2 \times 10^{17}$	$1 \times 10^{18}$	$2.02 \times 10^{17}$
Valence Band density of states, $N_V$ ( $\text{cm}^{-3}$ )	$1.8 \times 10^{19}$	$2.2 \times 10^{16}$	$1 \times 10^{18}$	$1.1 \times 10^{19}$
Electron thermal velocity, $V_e$ (cm/s)	$1 \times 10^7$	$1 \times 10^7$	$1 \times 10^7$	$1 \times 10^7$
Hole thermal velocity, $V_h$ (cm/s)	$1 \times 10^7$	$1 \times 10^7$	$1 \times 10^7$	$1 \times 10^7$
Electron mobility, $\mu_e$ ( $\text{cm}^2/\text{Vs}$ )	20	20	1.6	20
Hole mobility, $\mu_h$ ( $\text{cm}^2/\text{Vs}$ )	10	10	1.6	80
Density of donor, $N_D$ ( $\text{cm}^{-3}$ )	$2.0 \times 10^{19}$	* $1 \times 10^{17}$	0	0
Density of acceptor, $N_A$ ( $\text{cm}^{-3}$ )	0	0	$1 \times 10^{18}$	* $1 \times 10^{17}$



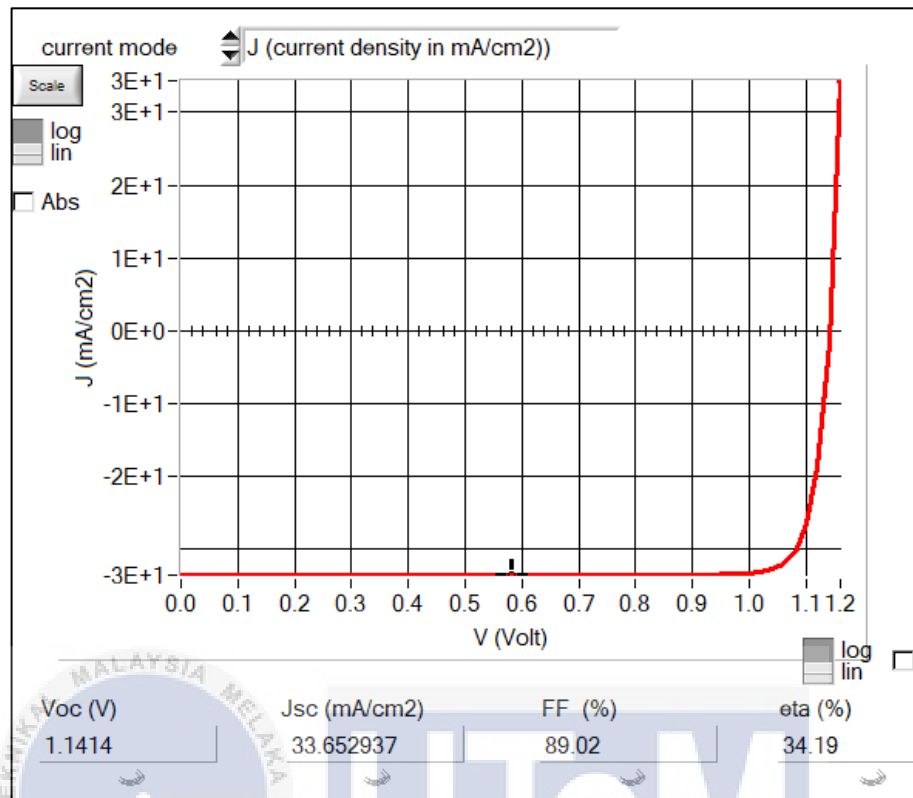


Figure 4.12: J-V curve for the optimized PSC structure using SnO<sub>2</sub> as an ETL.

The detailed analysis presented in Table 4.22 highlights the optimal efficiency achieved by incorporating SnO<sub>2</sub> as an electron transport layer (ETL) when all parameters are replaced with their respective optimal values. The simulation results show an impressive Power Conversion Efficiency (PCE) of 34.19%, which represents a significant improvement in overall performance. This improvement is further enhanced by a fill factor (FF) of 89.02%, indicating improved charge carrier transport efficiency within the solar cell. In addition, the open-circuit voltage (Voc) reaches a significant value of 1.141 V, highlighting the robust performance of the optimized structure. At the same time, the short-circuit current (Jsc) is 33.653 mA/cm<sup>2</sup>, indicating increased power generation in the solar cell. Overall, these results highlight the effectiveness of incorporating SnO<sub>2</sub> as an ETL and MASnI<sub>3</sub> as an absorber, not

only in improving the overall efficiency but also in improving critical parameters, which helps optimize the performance of perovskite solar cells (PSC).



## CHAPTER 5:

### CONCLUSION AND FUTURE WORKS



In this section will portray about conclusion and recommendation for the Investigation of Lead-Free Perovskite  $\text{MASnI}_3$  Based Solar Cells Using SCAPS Simulation. This section additionally incorporates project rundown, project finding and further proposal to improve the project.

## 5.1 Conclusion

In summary, the perovskite solar cell (PSC) is a promising representative of the third generation of solar cells, which consists of essential components such as the electron transport layer (ETL), the absorber and the hole transport layer (HTL). This study focused on the optimization of the lead-free PSC structure with MASnI<sub>3</sub> as absorber, TiO<sub>2</sub> and SnO<sub>2</sub> as ETLs, and conducted a comprehensive analysis using SCAPS-1D simulator. The simulation results for the FTO/TiO<sub>2</sub>/MASnI<sub>3</sub>/Cu<sub>2</sub>O configuration showed remarkable performance improvements. The power conversion efficiency (PCE) reached an impressive 34.41%, accompanied by a fill factor (FF) of 88.95%, highlighting the improved carrier transport efficiency. The open-circuit voltage (V<sub>oc</sub>) showed significant performance with a value of 1.142 V, and the short-circuit current (J<sub>sc</sub>) was 33.877 mA/cm<sup>2</sup>, indicating increased power generation in the solar cell.

Likewise, the simulation results for the FTO/SnO<sub>2</sub>/MASnI<sub>3</sub>/Cu<sub>2</sub>O configuration showed a significant improvement in overall performance. The power conversion efficiency (PCE) reached an impressive 34.19%, complemented by a fill factor (FF) of 89.02%, indicating improved carrier transport efficiency. The open circuit voltage (V<sub>oc</sub>) showed robust performance with a significant value of 1.141 V and the short circuit current (J<sub>sc</sub>) was recorded at 33.653 mA/cm<sup>2</sup>, indicating increased power generation in the solar cell. These results highlight the effectiveness of MASnI<sub>3</sub> as an absorber and the optimization of the PSC structure with TiO<sub>2</sub> and SnO<sub>2</sub> as ETLs. The study considered critical parameters such as working temperature, absorber thickness, doping density of ETL and HTL, and defect density at the ETL and absorber interface. The success of these simulations highlights the potential for further advances in PSC

technology and provides a path to more efficient and sustainable solar energy solutions.

## 5.2 Future Work

Looking forward, the insights gained from these simulation results hold promise as a blueprint for future manufacturing methods for lead-free perovskite solar cells. The use of TiO<sub>2</sub> and SnO<sub>2</sub> as electron transport layers (ETLs) alongside MASnI<sub>3</sub> as an absorber represents a compelling way to improve the efficiency of lead-free PSC. To further improve the lead-free PSC, optimizing the absorber thickness, minimizing the ETL thickness and the use of Cu<sub>2</sub>O as a hole transport layer material (HTL) can be investigated. These parameters, based on the simulation results, provide a practical roadmap for achieving superior performance in lead-free PSC manufacturing.

In addition, the simulation results serve as a valuable guide for the development and production of lead-free perovskite solar cells. By using MASnI<sub>3</sub> as absorber, TiO<sub>2</sub> and SnO<sub>2</sub> as ETLs and Cu<sub>2</sub>O as HTL, this innovative approach fits the growing importance of environmentally friendly and sustainable solar cell technologies. The simulation results provide crucial insights into the interaction of these materials and their impact on the performance metrics of lead-free perovskite solar cells. As the field continues to develop, these findings can help advance the understanding and practical implementation of lead-free alternatives and represent a significant step toward more sustainable and efficient solar energy solutions.

## REFERENCES

- [1] “Best research-cell efficiency chart,” NREL, <https://www.nrel.gov/pv/cell-efficiency.html> (accessed Jan. 8, 2024).
- [2] H. Aribisala, “Improving the efficiency of solar photovoltaic power system”. doi:10.23860/thesis-aribisala-henry-2013
- [3] J. L, “What is renewable energy? benefits, sources, and top companies,” Carbon Credits, <https://carboncredits.com/what-is-renewable-energy-benefits-sources-and-top-companies/> (accessed Dec. 30, 2023).
- [4] M. T. Kibria, A. Ahammed, and S. M. Sony, “A Review : Comparative studies on different generation solar cells technology,” *Env. Aspects.*, pp. 51–53, 2014.
- [5] M. E. Ragoussi and T. Torres, “New generation solar cells: Concepts, trends and perspectives,” *Chem. Commun.*, vol. 51, no. 19, pp. 3957–3972, 2015.
- [6] O. Vigil-Galán, M. Courel, and J. A. Andrade-Arvizu, “Route towards low costhigh efficiency second generation solar cells: current status and perspectives,” *J. Mater. Sci. Mater. Electron.*, vol. 26, no. 8, pp. 5562–5573, 2015

- [7] M. A. Green, "Third generation photovoltaics: Solar cells for 2020 and beyond," *Phys. E Low-Dimensional Syst. Nanostructures*, vol. 14, no. 1–2, pp. 65–70, 2002
- [8] J. Yan and B. R. Saunders, "Third-generation solar cells: A review and comparison of polymer:fullerene, hybrid polymer and perovskite solar cells," *RSC Adv.*, vol. 4, no. 82, pp. 43286–43314, 2014.
- [9] S. R.S. Shelke, "Status and Perspectives of Dyes Used in Dye Sensitized Solar Cells," *Int. J. Renew. Energy Resour. (formerly Int. J. Renew. Energy Res.)*, vol. Volume 3, no. Issue 2, pp. 54–61, 2014.
- [10] B. Osman, T. Abdolkader, and I. Ahmed, "A Review of Perovskite Solar Cells," *Int. J. Mater. Technol. Innov.*, 2021, doi: 10.21608/ijmti.2021.78369.1032.
- [11] P. Zhang *et al.*, "Perovskite Solar Cells with ZnO Electron-Transporting Materials," *Adv. Mater.*, vol. 30, no. 3, pp. 1–20, 2018, doi: 10.1002/adma.201703737.
- [12] J. Zhang *et al.*, "Multifunctional Molecule Engineered SnO<sub>2</sub> for Perovskite Solar Cells with High Efficiency and Reduced Lead Leakage," *Sol. RRL*, vol. 5, no. 10, pp. 1–10, 2021, doi: 10.1002/solr.202100464.
- [13] A. H. M. Smets, K. Jäger, O. Isabella, R. A. van Swaaij, and M. Zeman, "Solar Cell Parameters and Equivalent Circuit," *Sol. energy Phys. Eng. Photovolt. conversion, Technol. Syst.*, pp. 113–121, 2016.
- [14] B. Qi and J. Wang, "Fill factor in organic solar cells," *Phys. Chem. Chem. Phys.*, vol. 15, no. 23, pp. 8972–8982, 2013, doi: 10.1039/c3cp51383a.

- [15] H. Alipour and A. Ghadimi, "Optimization of lead-free perovskite solar cells in normal-structure with WO<sub>3</sub> and water-free PEDOT: PSS composite for hole transport layer by SCAPS-1D simulation," *Optical Materials*, vol. 120, p. 111432, 2021.
- [16] M. Vishnuwaran, K. Ramachandran, P. Roy, and A. khare, "SCAPS simulated FASNI<sub>3</sub> and masni<sub>3</sub> based PSC solar cells: A comparison of device performance," *IOP Conference Series: Materials Science and Engineering*, vol. 1219, no. 1, p. 012048, 2022.
- [17] A. K. Al-Mousoi *et al.*, "Simulation and analysis of lead-free perovskite solar cells incorporating cerium oxide as electron transporting layer," *RSC Advances*, vol. 12, no. 50, pp. 32365–32373, 2022. doi:10.1039/d2ra05957f
- [18] H. Abedini-Ahangarkola, S. Soleimani-Amiri, and S. Gholami Rudi, "Modeling and numerical simulation of high efficiency perovskite solar cell with three active layers," *Solar Energy*, vol. 236, pp. 724–732, 2022. doi:10.1016/j.solener.2022.03.055
- [19] K. Deepthi Jayan and V. Sebastian, "Comprehensive device modelling and performance analysis of MASnI<sub>3</sub> based perovskite solar cells with diverse etm, HTM and back metal contacts," *Solar Energy*, vol. 217, pp. 40–48, 2021.
- [20] A. K. Singh, S. Srivastava, A. Mahapatra, J. K. Baral, and B. Pradhan, "Performance optimization of lead free-MASNI<sub>3</sub> based solar cell with 27% efficiency by numerical simulation," *Optical Materials*, vol. 117, p. 111193, 2021.



- [21] A. Hima, “Enhancing of CH<sub>3</sub>NH<sub>3</sub>SnI<sub>3</sub> based solar cell efficiency by ETL Engineering,” *International Journal of Energetica*, vol. 5, no. 1, p. 27, 2020.
- [22] N. Singh, A. Agarwal, and M. Agarwal, “Numerical simulation of highly efficient lead-free all-perovskite tandem solar cell,” *Solar Energy*, vol. 208, pp. 399–410, 2020. doi:10.1016/j.solener.2020.08.003
- [23] T. Minemoto et al., “Theoretical Analysis of band alignment at Back Junction in sn–Ge perovskite solar cells with inverted P-i-N structure,” *Solar Energy Materials and Solar Cells*, vol. 206, p. 110268, 2020. doi:10.1016/j.solmat.2019.110268
- [24] A. Bouich, J. Marí-Guaita, B. M. Soucase, and P. Palacios, “Manufacture of high-efficiency and stable lead-free solar cells through antisolvent quenching engineering,” *Nanomaterials*, vol. 12, no. 17, p. 2901, 2022. doi:10.3390/nano12172901
- [25] F. Li et al., “TRIHYDRAZINE dihydriodide-assisted fabrication of Efficient Formamidinium Tin iodide perovskite solar cells,” *Solar RRL*, vol. 3, no. 9, p. 1900285, 2019. doi:10.1002/solr.201900285
- [26] P. Wang et al., “Ion Exchange/insertion reactions for fabrication of efficient methylammonium tin iodide perovskite solar cells,” *Advanced Science*, vol. 7, no. 9, p. 1903047, 2020. doi:10.1002/advs.201903047
- [27] B. P. Nguyen et al., “Phase formation and local charge transport of lead-free CH<sub>3</sub>NH<sub>3</sub>Sn(I<sub>1-x</sub>Br<sub>x</sub>)<sub>3</sub> (0 ≤ x ≤ 1) perovskite solar cells fabricated by solvent optimization,” *Solar Energy*, vol. 186, pp. 136–144, 2019. doi:10.1016/j.solener.2019.05.007

- [28] F. Li et al., “A cation-exchange approach for the fabrication of efficient methylammonium tin iodide perovskite solar cells,” *Angewandte Chemie International Edition*, vol. 58, no. 20, pp. 6688–6692, 2019. doi:10.1002/anie.201902418
- [29] Y. Yu et al., “Thermally evaporated methylammonium tin triiodide thin films for lead-free perovskite solar cell fabrication,” *RSC Advances*, vol. 6, no. 93, pp. 90248–90254, 2016. doi:10.1039/c6ra19476a
- [30] A. Kabalan and S. Roy, “Integrating solar cells simulation software in an Undergraduate Engineering Class,” *ASEE Mid-Atlantic Sect. Conf.*, pp. 1–10, 2016
- [31] M. Burgelman, J. Verschraegen, S. Degrave, and P. Nollet, “Modeling thin-film PV devices,” *Progress in Photovoltaics: Research and Applications*, vol. 12, no. 2–3, pp. 143–153, 2004. doi:10.1002/pip.524
- [32] T. M. Koh et al., “Formamidinium Tin-based perovskite with low  $E_g$  for photovoltaic applications,” *Journal of Materials Chemistry A*, vol. 3, no. 29, pp. 14996–15000, 2015. doi:10.1039/c5ta00190k
- [33] H.-J. Du, W.-C. Wang, and J.-Z. Zhu, “Device simulation of lead-free  $\text{CH}_3\text{NH}_3\text{SnI}_3$  perovskite solar cells with high efficiency,” *Chinese Physics B*, vol. 25, no. 10, p. 108802, 2016. doi:10.1088/1674-1056/25/10/108802
- [34] S. Bansal and P. Aryal, “Evaluation of new materials for electron and hole transport layers in perovskite-based solar cells through SCAPS-1D simulations,” *2016 IEEE 43rd Photovoltaic Specialists Conference (PVSC)*, 2016. doi:10.1109/pvsc.2016.7749702

- [35] C. Devi and R. Mehra, "Device simulation of lead-free MASNI<sub>3</sub> solar cell with CUSBS<sub>2</sub> (copper antimony sulfide)," *Journal of Materials Science*, vol. 54, no. 7, pp. 5615–5624, 2019. doi:10.1007/s10853-018-03265-y
- [36] M. Shasti and A. Mortezaali, "Numerical Study of Cu<sub>2</sub>O, SrCu<sub>2</sub>O<sub>2</sub>, and CuAlO<sub>2</sub> as hole-transport materials for application in perovskite solar cells," *physica status solidi (a)*, vol. 216, no. 18, 2019. doi:10.1002/pssa.201900337
- [37] P. K. Patel, "Device simulation of highly efficient eco-friendly CH<sub>3</sub>NH<sub>3</sub>SNI<sub>3</sub> perovskite solar cell," *Scientific Reports*, vol. 11, no. 1, 2021. doi:10.1038/s41598-021-82817-w
- [38] Y. Raoui et al., "Performance analysis of mapbi<sub>3</sub> based perovskite solar cells employing diverse charge selective contacts: Simulation study," *Solar Energy*, vol. 193, pp. 948–955, 2019. doi:10.1016/j.solener.2019.10.009
- [39] D. Dey, D. De, A. Ahmadian, F. Ghaemi, and N. Senu, "Electrically Doped Nanoscale Devices Using First-Principle Approach: A Comprehensive Survey," *Nanoscale Research Letters*, vol. 16, no. 1, 2021, doi: 10.1186/s11671-020-03467-x.
- [40] C. Mebarkia, D. Dib, H. Zerfaoui, and R. Belghit, "Energy efficiency of a photovoltaic cell based thin films CZTS by SCAPS," *J. Fundam. Appl. Sci.*, vol. 8, no. 2, p. 363, 2016, doi: 10.4314/jfas.v8i2.13.
- [41] K. B. Nine, M. F. Hossain, and S. A. Mahmood, "Analysis of Stable, Environment Friendly and Highly Efficient Perovskite Solar Cell," *IEEE*

*Reg. 10 Annu. Int. Conf. Proceedings/TENCON*, vol. 2019-October, pp. 1825–1828, 2019, doi: 10.1109/TENCON.2019.8929358.

- [42] A. Rahman, “Design and simulation of high-performance planar NPP+ heterojunction  $\text{CH}_3\text{NH}_3\text{PbI}_3$  based perovskite solar cells using  $\text{BaSnO}_3$  ETM and  $\text{Cu}_2\text{O}$  HTM”, 2021. doi:10.21203/rs.3.rs-441744/v1

